AD A061313

LEVEL II

AFFDL-TR-77-60

BIRD IMPACT FORCES AND PRESSURES ON RIGID AND COMPLIANT TARGETS

UNIVERSITY OF DAYTON
RESEARCH INSTITUTE
300 COLLEGE PARK AVENUE
DAYTON, OHIO 45469

MAY 1978

TECHNICAL REPORT AFFDL-TR-77-60
Final Report for Period April 1976 – December 1976

Approved for public release; distribution unlimited.

AIR FORCE FLIGHT DYNAMICS LABORATORY
AIR FORCE WRIGHT AERONAUTICAL LABORATORIES
AIR FORCE SYSTEMS COMMAND
WRIGHT-PATTERSON AIR FORCE BASE, OHIO 45433

78 10 30 076

NOTICE

This technical report has been reviewed and is approved for publication.

RICHARD L. PETERSON, Project Manager
Improved Windshield Protection ADPO
Vehicle Equipment Division
Air Force Flight Dynamics Laboratory

FOR THE COMMANDER

ROBERT E. WITTMAN, Program Manager
Improved Windshield Protection ADPO
Vehicle Equipment Division
Air Force Flight Dynamics Laboratory

AMBROSE B. NUTT
Director
Vehicle Equipment Division
Air Force Flight Dynamics Laboratory

AIR FORCE/56780/12 October 1973 — 150

LEVEL II

UNCLASSIFIED

SECURITY CLASSIFICATION OF THIS PAGE (When Data Entered)

REPORT DOCUMENTATION PAGE

READ INSTRUCTIONS BEFORE COMPLETING FORM

1. REPORT NUMBER: AFFDL-TR-77-60
2. GOVT ACCESSION NO.
3. RECIPIENT'S CATALOG NUMBER
4. TITLE (and Subtitle): BIRD IMPACT FORCES AND PRESSURES ON RIGID AND COMPLIANT TARGETS
5. TYPE OF REPORT & PERIOD COVERED: Final Report, April 1976 – December 1976
6. PERFORMING ORG. REPORT NUMBER: UDRI-TR-77-17
7. AUTHOR(s): John P. Barber, Henry R. Taylor, James S. Wilbeck
8. CONTRACT OR GRANT NUMBER(s): F33615-76-C-3103
9. PERFORMING ORGANIZATION NAME AND ADDRESS: University of Dayton Research Institute, 300 College Park Avenue, Dayton, Ohio 45469
10. PROGRAM ELEMENT, PROJECT, TASK AREA & WORK UNIT NUMBERS: Project No. 2202, Task No. 220203, Work Unit No. 22020305
11. CONTROLLING OFFICE NAME AND ADDRESS: Air Force Flight Dynamics Laboratory/FEW, Wright-Patterson Air Force Base, Ohio 45433
12. REPORT DATE: May 1978
13. NUMBER OF PAGES: 73
14. MONITORING AGENCY NAME & ADDRESS (if different from Controlling Office): 86p.
15. SECURITY CLASS. (of this report): UNCLASSIFIED

15a. DECLASSIFICATION DOWNGRADING SCHEDULE

16. DISTRIBUTION STATEMENT (of this Report): Approved for public release; distribution unlimited.
17. DISTRIBUTION STATEMENT (of the abstract entered in Block 20, if different from Report)

18. SUPPLEMENTARY NOTES
19. KEY WORDS (Continue on reverse side if necessary and identify by block number): Bird Impact, Impact Response, Birdstrike, Impact, Impact Loads
20. ABSTRACT (Continue on reverse side if necessary and identify by block number)

An experimental and analytical investigation of bird impact loading was conducted. Bird impact total forces were measured using a Hopkinson bar technique. A nondimensionalized description of the total force and its variation with time was developed from the data. Bird impact pressures were also measured. The impact event was found to consist of four processes. The first process is the initial shock phase in which extremely high pressures are generated. These pressures may be calculated if the Hugoniot relations for the bird material are known. It was found that gelatin with ten percent porosity

405 400

20. ABSTRACT (continued)

provided a good material model for the prediction of impact pressures. The second process is the impact shock decay phase. During this phase radial release waves propagate from the edges of the bird towards the center of impact. These radial release waves accelerate the bird material radially and attenuate the shock. The third impact process is a steady flow condition which follows the shock decay. During this phase the bird behaves like a jet flowing steadily onto the target. The final impact process is the termination and this occurs when the end of the bird reaches the target. Each of these processes was examined analytically and experimentally. Birds ranging in size from 60g to 4 kg were investigated. Impact angles of 90°, 45°, and 25° were employed. Impact velocities typical of aircraft/bird encounters (50 to over 300 m/s) were chosen. Birds were found to behave as a fluid during impact. All the important features of the impact process were successfully analyzed.

The effects of target compliance on bird loading were also investigated. Target compliance was divided into two classes, locally rigid and locally deforming. A computational scheme designed to properly couple the loading to the response for locally rigid targets was devised. An exploratory experimental study of locally deforming targets was undertaken. Some important features of locally deforming response were identified.

FOREWORD

The effort reported herein was conducted in the Impact Physics Group under the direction of the Aerospace Mechanics Division of the University of Dayton Research Institute, Dayton, Ohio, under Contract F33615-76-C-3103, for the Air Force Flight Dynamics Laboratory, Wright-Patterson Air Force Base, Ohio. Air Force administrative direction and technical support was provided by Mr. Richard L. Peterson, AFFDL/FEW, the Air Force Project Manager. The experimental portion of the work was conducted at the Impact Mechanics facilities of the Air Force Materials Laboratory, Wright-Patterson Air Force Base, Ohio. The large bird testing was performed at Arnold Engineering Development Center, Arnold Air Force Station, Tennessee.

The work described herein was conducted during the period from May 1976 to December 1976. The principal investigator was Dr. John P. Barber, Head, Impact Physics Group of the Applied Physics Division of the University of Dayton Research Institute. Project supervision and technical assistance was provided through the Aerospace Mechanics Division of the University of Dayton Research Institute with Mr. Dale H. Whitford, Supervisor, Mr. George J. Roth, Leader, Structural Analysis Group, Blaine S. West, Project Engineer.

In addition to those listed above, the authors wish to acknowledge the following persons who made significant contributions to this work, Dr. David L. Quam/UDRI, Dr. Louis I. Boehman/UDRI, Mrs. Sue C. Gainor/UDRI.

The active support of the Air Force Materials Laboratory on this project is gratefully acknowledged. The complete cooperation of Dr. Ted Nicholas, AFML/LLN, and full use of the AFML Impact Mechanics Facility were required to successfully complete this project.

TABLE OF CONTENTS

SECTION		PAGE
I	INTRODUCTION	1
	1.1 Background	1
	1.2 The Bird Impact Loading Program	2
II	THE TOTAL FORCE IN BIRD IMPACTS	5
	2.1 Experimental Techniques	5
	2.2 Theoretical Considerations	12
	2.3 Experimental Results	15
	2.4 Summary	19
III	BIRD IMPACT PRESSURES	20
	3.1 Experimental Techniques	20
	3.2 Theoretical Considerations	23
	3.3 Experimental Results	40
	3.4 Summary	46
IV	EFFECTS OF TARGET COMPLIANCE ON BIRD LOADING	49
	4.1 Locally Rigid Windshield Response	50
	4.2 Locally Deforming Response	56
V	CONCLUSIONS AND RECOMMENDATIONS	70
	5.1 Conclusions	70
	5.2 Recommendations	71
	APPENDIX A	
	REFERENCES	

LIST OF ILLUSTRATIONS

FIGURE		PAGE
1.	The breech end of the compressed air driven launcher.	6
2.	Typical sabots for bird launching.	7
3.	The sabot stripper assembly.	8
4.	An x-radiograph of a bird in flight.	9
5.	The Hopkinson bar.	10
6.	Oblique Hopkinson bar configurations (a) tilted (b) sliced.	11
7.	A typical Hopkinson bar strain record.	12
8.	Motion of a bird before and after impact.	13
9.	Oblique impact effective bird length.	14
10.	Nondimensionalized impulse versus impact velocity for birds tested.	15
11.	Normalized impact duration versus impact velocity.	16
12.	Peak force versus impact velocity.	17
13.	Nondimensional rise time versus impact velocity.	18
14.	Generalized bird impact force-time profile.	19
15.	The AFML/UDRI pressure plate.	22
16.	The AEDC pressure plate and target area.	22
17.	A typical bird impact pressure record.	23
18.	The phases of bird impact (a) initial impact (b) impact decay (c) steady flow (d) termination.	25
19.	The shock pressure for birds[6] (gelatin with 10 percent porosity.)	26
20.	An oblique impact.	27
21.	The variation of bird impact pressure with impact angle. (Gelatin with 10 percent porosity.)	27
22.	Shock and release in a bird impact.	28
23.	Shock release time versus impact velocity for birds (Gelatin with 10 percent porosity.)	29
24.	Variation of critical length with impact velocity for birds (Gelatin with 10 percent porosity.)	31
25.	Steady state velocity.	33

FIGURE		PAGE
26.	Normal impact pressure distribution for birds (Gelatin with 10 percent porosity.)	33
27.	Oblique impact.	34
28.	Oblique impact potential flow model.	36
29.	Pressure coefficient ($2P/\rho v^2$)versus nondimensional radius along the major axis of the impact for oblique impacts.	39
30.	Initial impact (Hugoniot) pressures versus impact velocity for normal impact.	41
31.	Initial impact (Hugoniot) pressures versus impact velocity for 45° impacts.	42
32.	Steady flow pressures versus impact velocity at center of impact for 90° normal impacts.	43
33.	Steady flow nondimensional pressure distribution for normal impacts.	44
34.	Steady flow nondimensional pressure distribution along the major axis for oblique impact.	45
35.	Steady flow nondimensional pressure distribution along the minor axis for oblique impact.	45
36.	Nondimensional duration versus impact velocity for normal impacts.	47
37.	Locally rigid windshield response.	49
38.	Locally deforming windshield response.	50
39.	The geometry of a locally rigid impact.	51
40.	Nondimensional impact area versus nondimensional consumed length.	53
41.	A locally deforming target.	57
42.	A Hopkinson tube.	58
43.	The Hopkinson tube in place.	59
44.	Nondimensional impulse transfer versus impact velocity for normal impact.	61
45.	Nondimensional impact duration versus impact velocity for normal impact.	62
46.	Nondimensional peak force versus impact velocity for normal impact.	63

LIST OF ILLUSTRATIONS (cont'd)

FIGURE		PAGE
47.	Nondimensional rise time versus impact velocity for normal impact.	64
48.	Rise time divided by the time to peak displacement versus impact velocity for normal impact.	64
49.	Impulse transfer versus impact momentum for 45° impacts.	65
50.	Nondimensionalized pulse duration versus impact velocity for 45° impacts.	66
51.	Nondimensionalized peak force versus impact velocity for 45° impacts.	67
52.	Nondimensional rise time versus impact velocity for 45° impacts.	68
53.	Rise time divided by time to peak displacement versus velocity for 45° impacts.	68

SECTION I
INTRODUCTION

Birds and aircraft occupy the same air space and collisions between the two are inevitable. As aircraft speeds have increased, the severity and importance of bird/aircraft impact have also increased. As a result, efforts have been made to reduce the probability of collision by controlling the movement of birds and by changing the flight paths of aircraft. These actions can and have reduced the probability of collision but have not eliminated it. Therefore, the Air Force has initiated programs designed to increase birdstrike resistance of aircraft and aircraft components. This report describes a program which was conducted to establish the loads which birds exert on aircraft transparencies in collisions. The loads as derived in this program were to be used as input for the structural analysis computer code of windshield response to bird impact.

1.1 BACKGROUND

Studies of the hazards presented by bird impact on transparencies date back to the early 1940's. Since that time the potential damage resulting from bird/aircraft collisions has greatly increased. This is principally the result of increased aircraft speeds which results in both increased energy densities and impulsive forces during the impact process. The problem has been further aggravated by the introduction of low altitude, high speed penetration, mission profiles. These flight profiles place the aircraft in areas of high bird density at speeds approaching or exceeding the speed of sound. Birdstrikes under these conditions increase the probability of serious aircraft damage. Such damage may result in an aborted mission or loss of aircraft.

Since 1966 the U.S. Air Force has lost at least twelve aircraft worth over $76 million due to bird impacts on transparent enclosures. These losses include a T-37B with one fatality, three T-38s with two fatalities, two F-100s with one fatality, and six F-111s with two fatalities. In addition to the $76 million loss in airframes, an estimated $20 million has been spent in repair costs during the period 1966 through 1972. Further, the role of bird impacts in aircraft losses in Southeast Asia is not fully known.

Numerous efforts are currently underway to make U.S. Air Force aircraft windshield systems more resistant to bird impacts. In addition, a number of advanced development programs are being conducted to examine existing windshield materials and birdstrike resistance windshield system concepts. It has become apparent from these studies that the technological base developed during the 1940s, 50s, and early 60s for birdstrike resistance is not adequate. Current improved designs are principally arrived at with an inefficient and expensive build and test process.

The design of birdstrike resistant transparencies requires a better and more detailed knowledge of the response of windshields and support structures to bird impact. The Air Force has initiated an extensive program which is designed to apply modern structural analysis techniques to windshield response. With such tools proven and placed at the designers disposal, the process of obtaining birdstrike resistant transparency designs should become much more efficient.

One of the most important inputs to a structural analysis code is the loading. The loading is particularly important in the analysis of transient response such as occurs in bird impact. The program described in this report was designed to support the structural analysis tasks by providing experimentally obtained and quantified loading input data.

1.2 THE BIRD IMPACT LOADING PROGRAM

The effort to measure and characterize the loads exerted by birds during impact was begun in January 1974. This work was jointly sponsored by the Air Force Materials Laboratory and the Air Force Flight Dynamics Laboratory. The early work was reported by Barber, et al.[1]. In that phase of the program the basic experimental techniques required to obtain valid bird impact pressure data were developed. Bird launching techniques were established and tested. A technique employing quartz piezoelectric transducers were developed for measuring the impact pressures. These transducers were extensively tested and calibrated to assure the validity of the results. A preliminary series of bird impact tests were run with two bird sizes, 50 and 120 grams, investigated. Impacts at normal incidence were conducted at velocities ranging from < 50 m/s to ∿300 m/s. The basic nonsteady fluid dynamic behavior of birds in impact was identified. The basic characteristics of the pressure records were also identified and preliminary data reduction, analysis, and correlation were conducted.

The preliminary work reported in Reference 1 established the technique for measuring pressures and pointed to the need for direct measurements of the total impact force. Accordingly, the next phase of the program involved implementation of the Hopkinson bar technique to obtain total force measurements. In addition, the impact pressure measurements were extended to oblique impacts. Data was obtained at both 45° and 25° impact obliquity. This work was reported in detail by Peterson and Barber[2]. This report describes the successful development of the Hopkinson bar technique for total force measurements and reports the first series of total force results for normal impact. Bird impact pressure data at 45° and 25° was also presented. The reduction and analysis of the pressure data was significantly improved over the first report. The identification of a steady flow regime during the impact significantly improved the interpretation of the results. Spatial distribution of the steady flow pressures was documented.

Peterson and Barber[2] reported the first attempts to quantitatively reduce and analyze the bird pressure data obtained for large birds at Arnold Engineering Development Center (AEDC)[3]. This data had many puzzling characteristics which were quite unlike the AFML/UDRI data. Attempts to reduce and compare the AEDC data to the AFML/UDRI data were largely unsuccessful due to the fundamentally different nature of the pressure records. For example, with few exceptions, no steady pressure regime could be identified on the AEDC records. Some apparently valid measurements of total impulse and average pressures were obtained and these were consistent with the AFML/UDRI results and with the emerging physical picture of the impact process.

The current effort was designed to extend the work reported in Reference 2. The Hopkinson bar total force measurements were extended to oblique impacts at 45° and 25°, and to larger birds (600 g). The data base for total force measurements now covers a range of parameters as follows: bird masses ranging from 60 g to 600 g; impact velocities from < 100 m/s to ∿ 300 m/s; and impact obliquities of 90°, 45°, and 25°. A careful analysis of this body of data was conducted and the results are documented in this report.

In the current effort, measurements of impact pressures were extended to larger birds (600 g) in an effort to establish the size scaling laws of the impact process. In addition, the AEDC pressure data was once again reviewed in an attempt to determine the origin of the apparent descrepancies. The results of this effort are reported in Section III of this report.

All of the testing conducted in this program as described to this point were conducted on rigid targets. However, aircraft windshields are not rigid. The compliance of aircraft transparencies varies from almost rigid to extremely flexible. If this entire range of aircraft transparency compliances must be accommodated by analytic techniques then the effects of target motion on impact loading must be known. Therefore, in the current investigation on a preliminary study of the effects of target compliance on bird loading was undertaken. The results are reported in Section IV.

It was recognized early in the program that bird loading data was not completely satisfactory as input into structural response codes. It is necessary to reduce that data or characterize it in a form which is more readily amenable to code input. In short, an analytic model of the bird impact process is required. Under the current program the task of establishing a reliable and verified analytic bird model was begun. This model is described in a separate report by Ito, et al.[4].

This report describes the output of the entire bird loading program and contains substantial portions of the work reported in References 1 and 2. The results of all phases of the program are integrated to provide a single, coherent report.

SECTION II

THE TOTAL FORCE IN BIRD IMPACTS

The total force which a bird exerts at impact is a very important parameter. In many cases, the response of an impacted structure can be adequately analyzed if the total impact force and its variation with time are known. In fact, a further simplification is often possible. If the natural period of the impacted structure is long compared with the duration of the impact, the impact may be considered to be an impulsive event. The only parameter required to adequately analyze the response is the impulse. Thus, if the variation of the total force with time is known (and the impulse, which is simply the integral of the force with time) a wide range of impact structural response problems may be analyzed. Many aircraft windshield bird collisions fall into this category. Accordingly, an extensive experimental program was undertaken to measure the total force exerted by birds at impact. This program was designed to yield information on the forces that birds exert and the manner in which those forces vary with time during impact. The results were cast in a form suitable for use with structural analysis programs.

This section contains a description of the experimental techniques used to measure the forces, some theoretical considerations of the forces and impulses delivered by birds at impact, and finally describes the experimental results.

2.1 EXPERIMENTAL TECHNIQUES

In order to study the forces exerted by birds at impact, birds must first be launched to velocities of interest. A suitably instrumented target must then be constructed and measurements of the forces obtained. A compressed air launching technique was developed and a Hopkinson bar was adapted to obtain measurements of the impact force and its variation with time.

2.1.1 The Launcher

For experimental investigations of bird impact, a launch technique is necessary which: (a) can launch birds of the required mass at the required velocities; (b) launches the birds with a controlled orientation (preferably with zero pitch and yaw); (c) does not break-up the bird or severely distort it prior to impact. A launch technique was developed with which birds of up to 700 g could be launched to velocities up to 300 m/s.

The launch tube was an 88.9 mm ID, 3.66 m long steel tube. Driving pressure was supplied by compressed air which was stored in a 0.32 m^3 steel tank. The maximum driving pressure available was 2.1 MN/m^2 (300 psi). The compressed air tank was connected to the breech of the gun with a 10 cm ID flexible hose and quick disconnect coupler. Gas was valved to the launch tube breech through a quick acting butterfly valve. The breech end of the gun, together with the flexible coupler and the gas storage tank, are shown in Figure 1.

The birds were placed in a sabot (carrier) for launching. The sabot was an 88.9 mm OD balsa wood cylinder. Balsa wood was employed because it is lightweight, strong, and relatively inexpensive. A suitable cavity was machined in the front of the sabot to accept the bird which was to be launched. A 38 mm cavity accommodated birds of about 60 g mass, while the maximum size bird launchable in this facility (600 g) required a 76 mm diameter cavity. A photograph of typical sabots is shown in Figure 2.

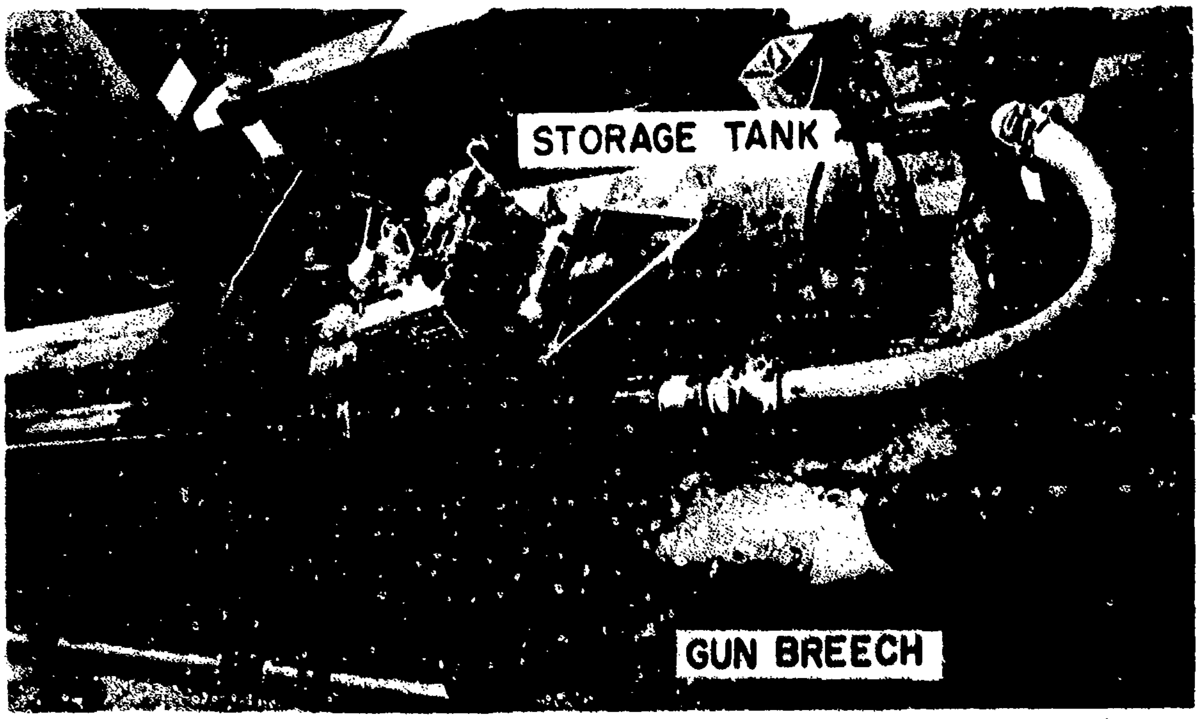

Figure 1. The breech end of the compressed air driven launcher.

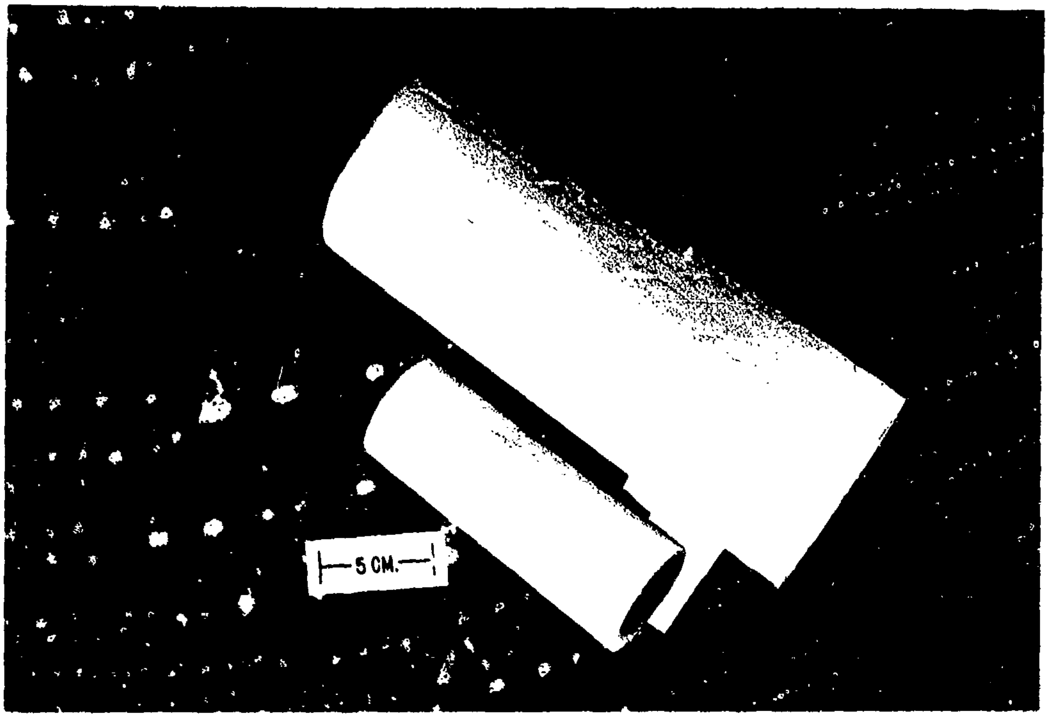

Figure 2. Typical sabots for bird launching.

These sabots proved completely satisfactory for launching birds over the range of sizes and velocities used in this study.

As the sabot represents a significant fraction of the launch mass, it must be stripped from the bird before the bird impacts the target. Accordingly, a sabot stripper section was attached to the muzzle of the launcher. The sabot stripper tube consisted of an 88.9 ID steel tube with a series of longitudinal slits cut into it. Compression rings were placed around the outside of the tube and ID of the tube was progressively reduced. When the launch package entered the sabot stripper tube, the sabot was progressively decelerated and finally stopped by the tube taper. The bird, however, released from the sabot pocket and continued free of the sabot to the target. Wide slots were cut in the muzzle of the launch tube to facilitate rapid release of the driving pressure and reduce the forces required to decelerate and stop the sabot. A photograph of the sabot stripper assembly is shown in Figure 3. In order to stop the high velocity large bird sabots an extension to the stipper tube is required. The tube could be extended from its standard length of 3.05 m to a total length of 4.88 m. The sabot stripper functioned satisfactorily over the entire range of masses and velocities which were used in this program.

Figure 3. The sabot stripper assembly.

The velocity of the bird was measured prior to impact using a simple time-of-flight technique. Between the muzzle of the sabot stripper and the target, two helium/neon laser beams were directed across the trajectory. When the bird interrupted the first laser beam, a counter was started. The counter was stopped when the bird interrupted the second laser beam. The distance between the laser beams and the elapsed time were used to calculate the velocity. To increase the accuracy of the velocity measurements and to monitor bird orientation and integrity prior to impact, a flash x-ray system was set up at each laser beam station. The resulting radiograph of the bird in flight was used to accurately establish the position of the bird with respect to the laser beam and to monitor the condition and orientation of the bird. A typical x-radiograph of a bird is shown in Figure 4. Using this technique, velocities could be measured to within one percent. Bird orientation and integrity were monitored for each shot. Bird disintegration during the free flight phase of the bird launch was extremely rare and was not an experimental problem. Birds were launched with an angle of attack (yaw) typically $< 5°$ to trajectory. The birds were always launched tail first for increased stability.

In addition to the x-radiograph coverage of the bird in flight, high speed motion picture coverage was also obtained on selected shots. Cameras with framing rates of up to 20,000 f/s were employed for specific investigations of the behavior of the bird during impact.

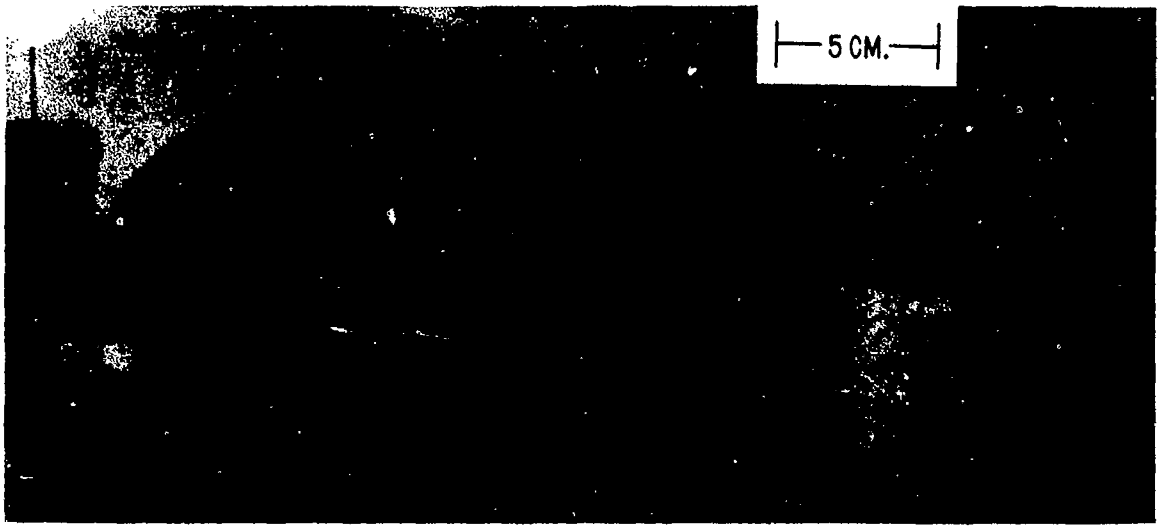

Figure 4. An x-radiograph of a bird in flight.

2.1.2 The Hopkinson Bar

Hopkinson bars have been used over the last fifty years for measuring force-time histories of impulsive events. The basic concept for which a Hopkinson bar operates is that a force rapidly applied to the end of a homogeneous bar of elastic material will generate a stress wave that propagates along the bar at constant (near sonic) velocity. The stress wave can be detected at any point along the bar by placing a strain gage on the bar surface and monitoring the output. The strain-time history is related to the instantaneous force applied to the end of the bar through the Young's modulus of the bar material and the cross-sectional area of the bar. The force is simply equal to the product of the strain, the modulus, and the cross-sectional area.

The Hopkinson bar principle was applied to determine the force-time history of a bird striking a rigid target. The birds were launched against the end of a long aluminum bar on which strain gages were mounted approximately ten diameters from the impact end. The resulting strain pulse in the bar was recorded and related to the force exerted by the impact. The bar must be sufficiently long to ensure that the entire stress pulse from the impact is recorded before a reflected wave from the free end of the bar can propagate back to the strain gage. Two separate bars were used in this investigation. For small birds (60 g) a 7.62 cm diameter, 3.66 m long aluminum bar was employed. Two strain gages were mounted on opposite sides of the bar, 76 cm from the impact end. For medium size birds (600 g) a

12.70 cm diameter bar, 4.83 m long with gages 1.25 m from the impacted end was used. The two gages were connected in opposite sides of a Wheatstone strain gage bridge for two purposes. This technique adds the output of the gages, thus doubling the sensitivity of the system. Any bending of the rod produces compression in one gage and tension in the other. These signals subtract and the bending signal is rejected. The signals were recorded with an oscilloscope.

The bar was located on the range by suspending it from the ceiling. Any perturbations to the strain signals which might be introduced by rigidly mounting the bar on the range were thus avoided. A photograph of the Hopkinson bar in place is shown in Figure 5.

Neglecting friction, an impacting bird can only exert forces which are normal to the impacted surface. For a normal impact on a Hopkinson bar, the impact force produces a planar strain wave which travels normal to the bar axis. The force as derived from the strain measurements is, therefore, exactly equal to the force exerted on the end of the bar. In oblique impact the situation is somewhat different.

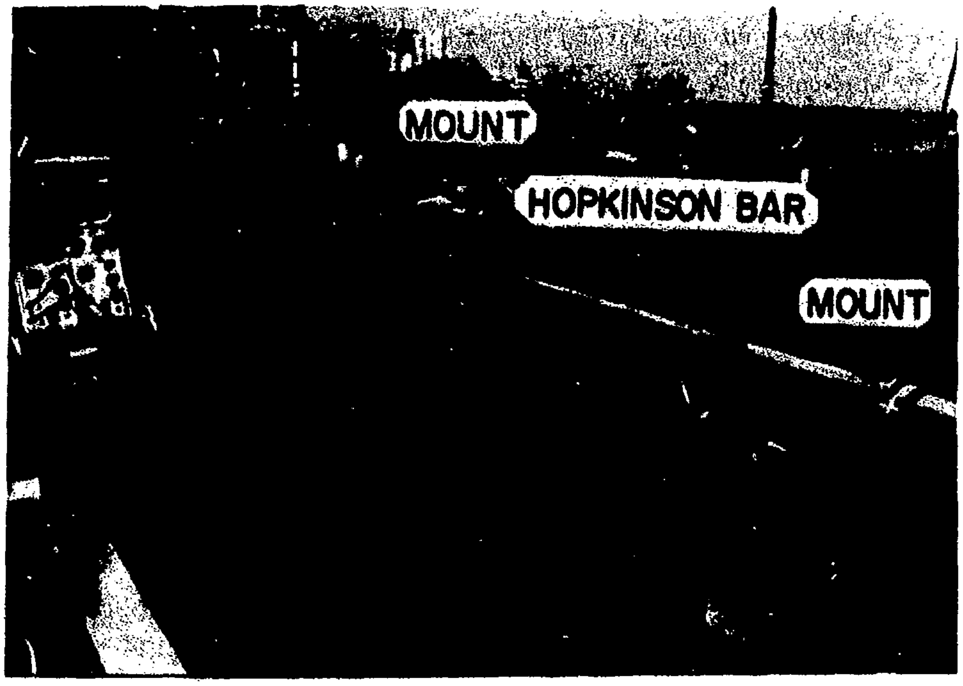

Figure 5. The Hopkinson bar.

A Hopkinson bar may be employed to investigate oblique impacts in one of two different modes. These modes are illustrated in Figure 6. In the tilted configuration the axis of the bar is tilted with respect to the trajectory of the bird. The impact forces are exerted normal to the surface of the end of the bar. As the end of the bar is perpendicular to the axis of the bar, the resulting strain wave propagates up the bar. The force derived from the strain measurements is exactly equal to the force exerted on the end of the bar.

When a sliced Hopkinson bar is employed to investigate oblique impacts, the force exerted by the impact is not directed along the axis of the bar. Only the component of the force which is parallel to the axis of the bar is detected by the strain gages. Both tilted and sliced bars were used in this study. The results from both configurations agree when they are appropriately reduced and analyzed.

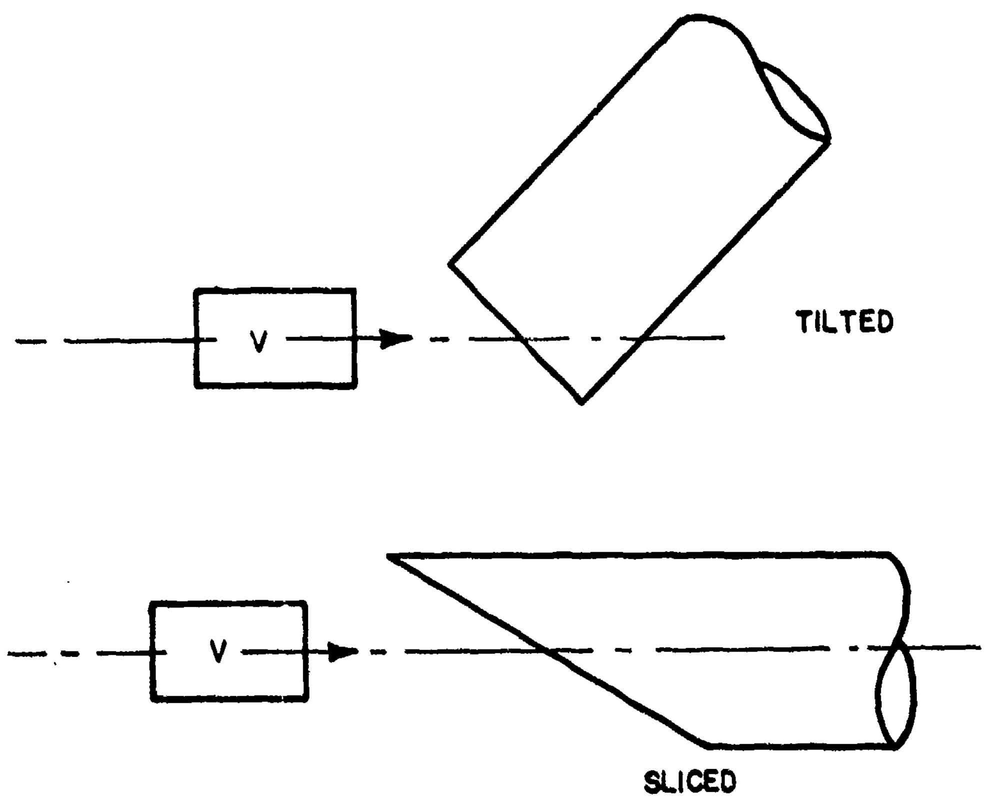

Figure 6. Oblique Hopkinson bar configurations (a) tilted (b) sliced.

A typical strain-time record is shown in Figure 7. The initial strain signal and the first two reflected signals are clearly visible. Only the primary strain signal was of interest.

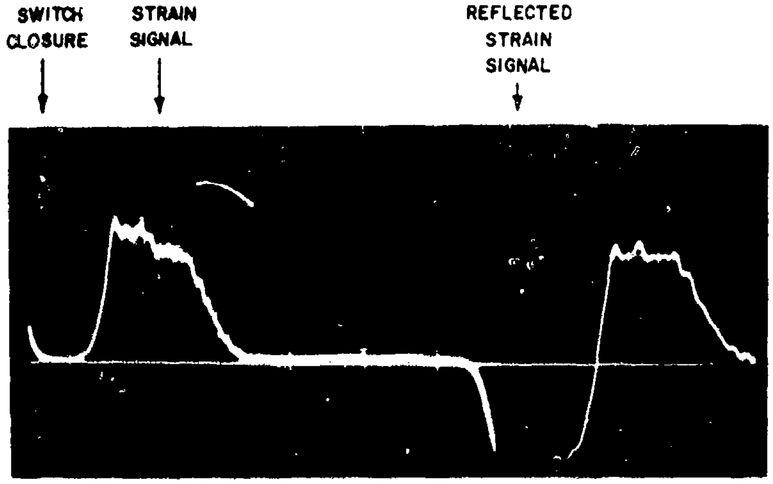

Figure 7. A typical Hopkinson bar strain record.

2.2 THEORETICAL CONSIDERATIONS

It is informative to consider some simple, theoretical results concerning impulse transfer, impact durations, and average forces in bird impacts. Knowledge of these qualities assists in the reduction and interpretation of experimental data.

2.2.1 Momentum Transfer

Assuming that a bird is essentially a fluid body, the motion of the bird before and after impact is illustrated in Figure 8. The initial momentum of the bird along trajectory is simply mv, where m is the mass of the bird and v is the initial impact velocity of the bird. The momentum of the bird along trajectory after impact is zero as the bird has only radial velocity. Therefore, the momentum transferred to the target during the impact is simply equal to mv. This simple picture may be easily extended to oblique impacts by noting that only the component of momentum normal to the impact surface is transferred to the target during the impact. Therefore, the momentum transfer, or impulse, I, is given by

$$I = mv \sin \Theta, \qquad (1)$$

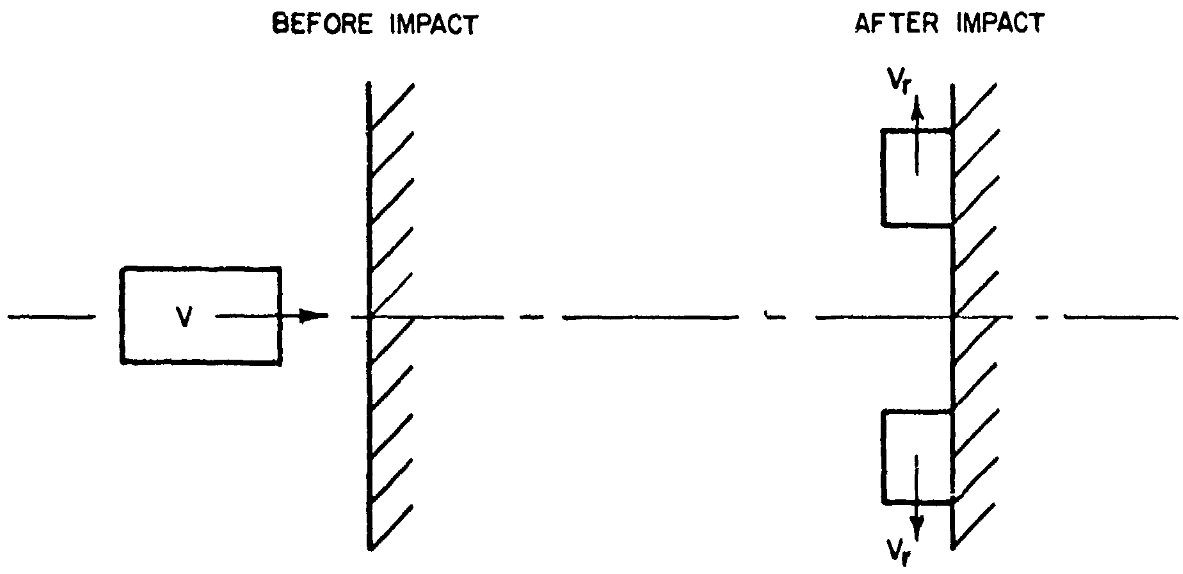

Figure 8. Motion of a bird before and after impact.

where Θ is the angle between trajectory and the surface of the target. Equation (1) is an expression for the momentum transfer or impulse imparted to a target during impact if the bird were a fluid body and the target were completely rigid.

2.2.2 Impact Duration

If the bird is assumed to be a fluid body, the impact begins when the leading edge of the bird first touches the target. The impact continues until the trailing edge reaches the target and there is no further bird material flowing onto the target. If the bird does not decelerate during impact, then this "squash-up time", T_s, is given by

$$T_s = \ell/v, \tag{2}$$

where ℓ is the length of the bird. In an oblique impact the situation is different as illustrated in Figure 9. The effective length of the bird is now somewhat longer than the "straight" length of the bird, ℓ. If the bird were a right circular cylinder, as illustrated in Figure 9, the effective length, ℓ_{eff}, would be given by

$$\ell_{eff} = \ell + d \tan \Theta \tag{3}$$

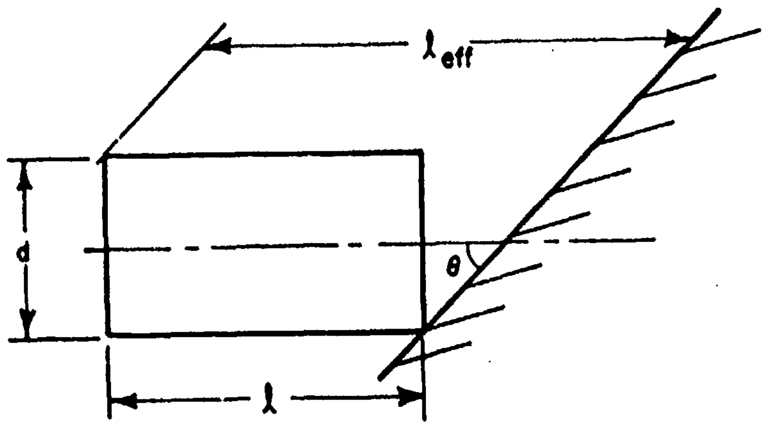

Figure 9. Oblique impact effective bird length.

where d is the diameter of the bird. A real bird is more nearly an oblate spheroid, in which case the effective length is less than that given by Equation (3). However, when the straight length is replaced by the effective length in Equation (2), a reasonable estimate of the pulse duration for an oblique impact is obtained.

2.2.3 Average Impact Force

Continuing the consideration of a fluid bird impact, both the momentum transfer and the duration have now been defined. With these two quantities it is possible to calculate the average impact force. The average force is given by the momentum transfer, Equation (1), divided by the duration

$$F_{avg} = mv^2 (\sin \theta) \ell_{eff} \tag{4}$$

The three quantities derived in this section, impulse, impact duration, and average impact force, are logical parameters with which to compare measured values and with which measured values can be nondimensionalized, or scaled, for presentation.

2.3 EXPERIMENTAL RESULTS

Impact experiments on Hopkinson bars were conducted over a wide range of bird impact parameters. Bird mass was varied from 60 g to 600 g. Impact velocity was varied from 50 m/s to 300 m/s. Three impact angles were investigated, 90° (normal), 45°, and 25°. Strain-time records were obtained for each impact. The strain-time records were converted to force-time records and from these records peak force, impact duration, and the rise time (time to reach peak force) were measured. In addition, the records were digitized and numerically integrated to provide data on momentum transfer or impulse. Details of the results are presented in the following sections.

2.3.1 Momentum Transfer

The momentum transfer or impulse which is determined by integrating the force-time records is compared to the momentum transfer as calculated in Section 2.2, Equation (1). The results are displayed in Figure 10. Figure 10 clearly demonstrates that Equation (1) contains all the essential characteristics of the momentum transfer. The equation properly scales for bird size, impact velocity, and impact angle. Birds appear to behave essentially as a fluid body. There is no evidence that bira. bounce at any velocity (which would imply an impulse greater than the expected momentum transfer).

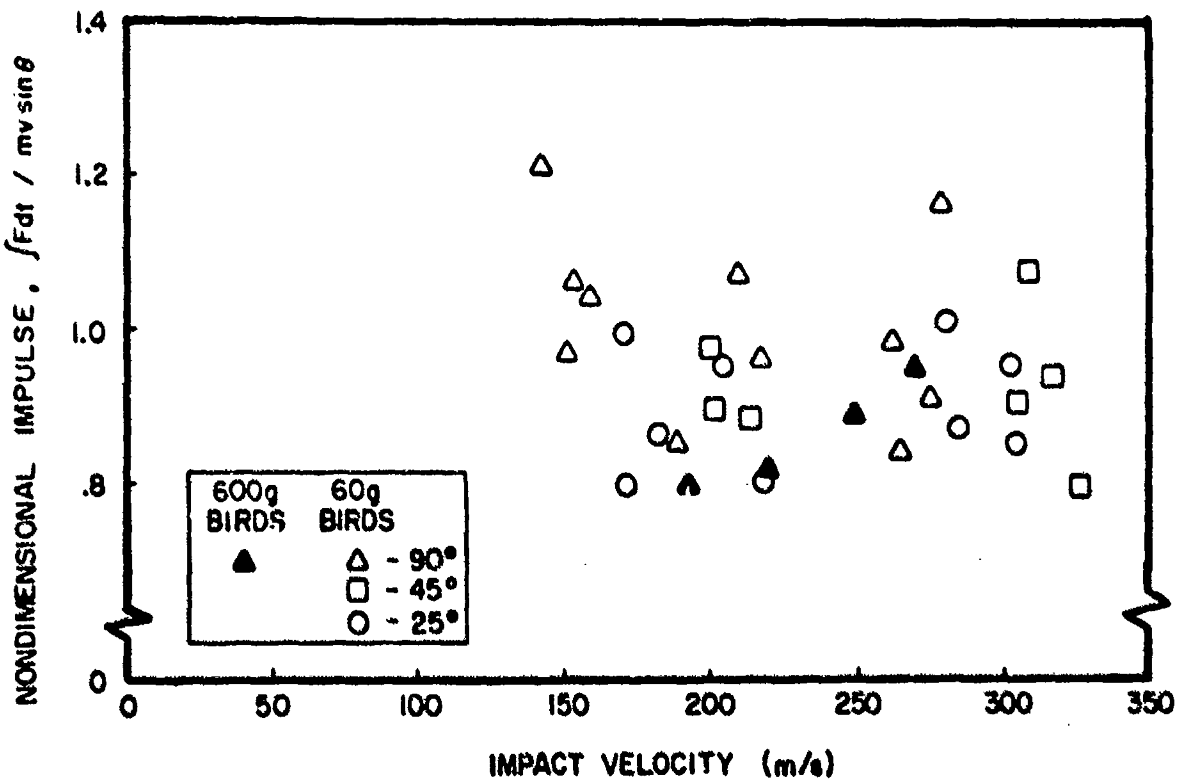

Figure 10. Nondimensionalized impulse versus impact velocity for birds tested.

2.3.2 Impact Duration

Impact durations were measured for most of the tests made. The impact duration was nondimensionalized to the "squash-up" time as given by Equations (2) and (3), and the results are displayed in Figure 11. From Figure 11 it is apparent that Equations (2) and (3) adequately describe the impact duration over a wide range of impact parameters. These expressions properly account for bird dimensions and impact velocities. The impact duration appears to scale linearly with size. The oblique impact results show a tendency for the measured duration to be less than the predicted "squash-up" time. This is due to the expression used to calculate the effective "squash-up" time, Equation (3), which assumes a right circular cylindrical shape. As birds are oblate spheroids, the effective length and "squash-up" time will be somewhat less than this value.

2.3.3 Peak Impact Force

The peak force recorded during each impact was evaluated and normalized to the average force as calculated from Equation (4). The results are displayed in Figure 12. There is considerable scatter in the

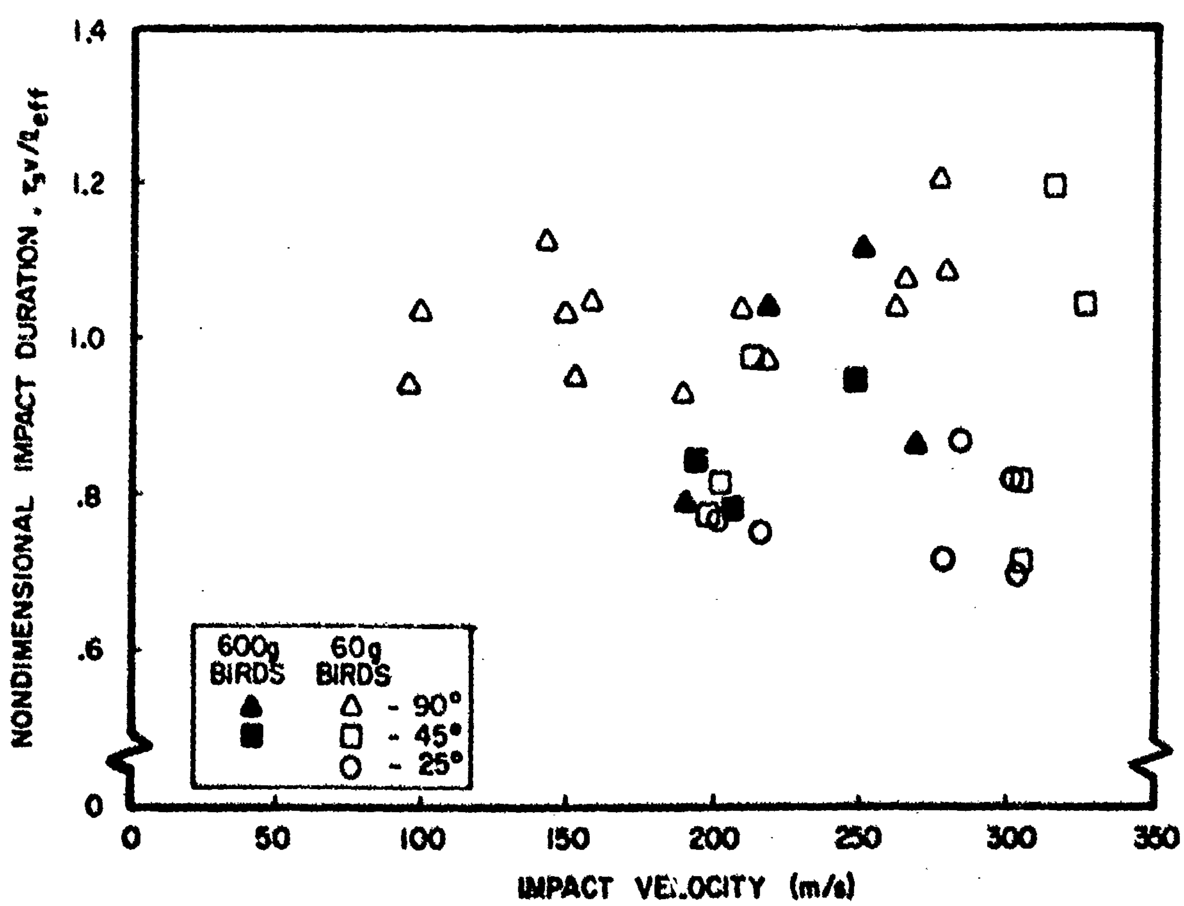

Figure 11. Normalized impact duration versus impact velocity.

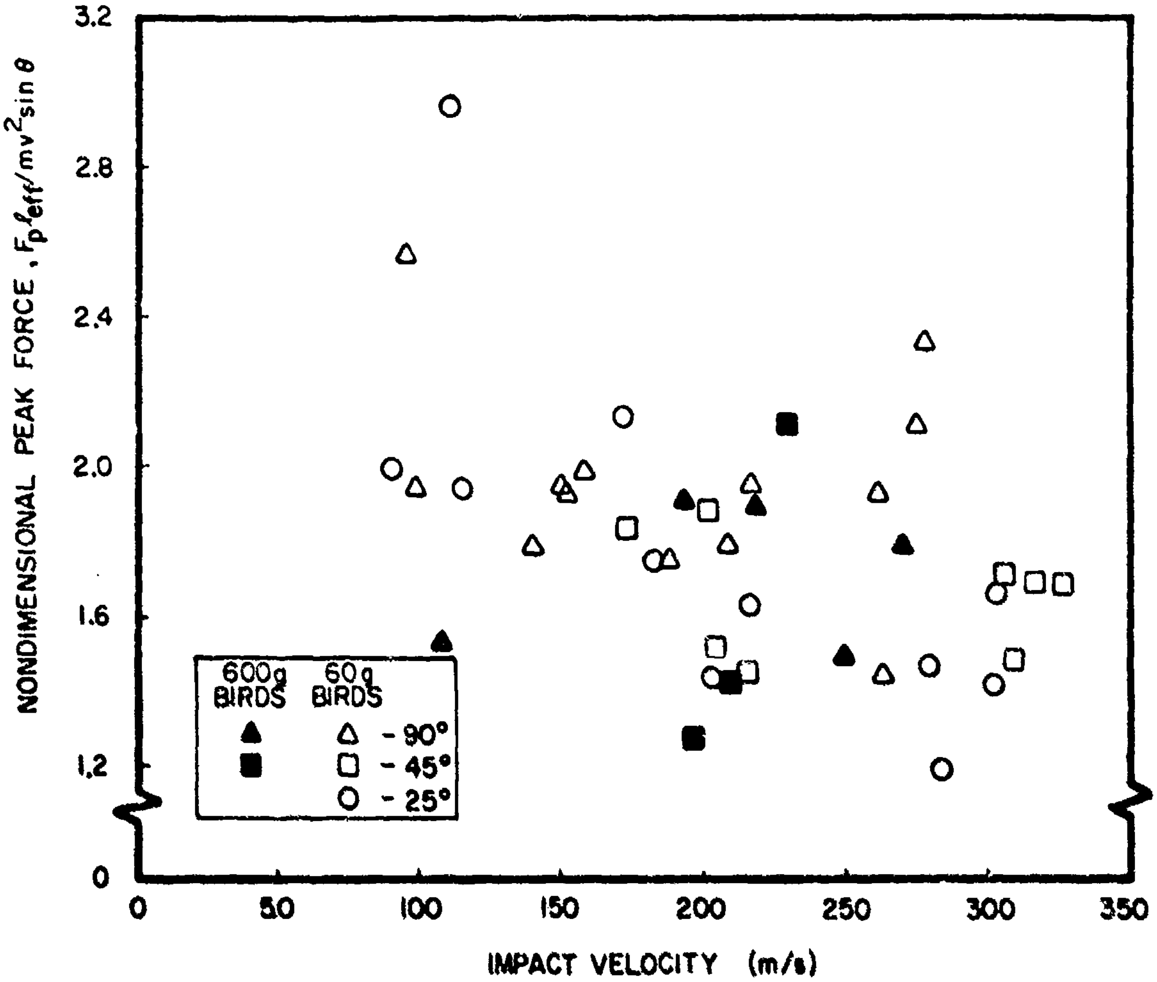

Figure 12. Peak force versus impact velocity.

data and this probably represents real variation in the forces exerted by birds at impact. The variation could be due to bird shape, bird material properties, and bird orientation at impact. The data appears to fall from a value of about 2 (e.g., the peak force is twice the average force) at 100 m/s to a value of about 1.6 at 300 m/s. There does not appear to be any significant difference between the 60 g birds and the 600 g birds. The average force, as determined from Equation (4), appears to be a good non-dimensionalizing parameter. A value of 2.0 leads to a simple "triangular" force-time distribution, is consistent within the data scatter, and represents a good "average" value.

2.3.4 Impact Rise Time

The impact rise time was taken to be the time from the beginning of impact until peak force was reached. This value was measured for all impacts and normalized to the "squash-up" time as derived from Equations (2) and (3). The results are displayed in Figure 13. There is a great deal of scatter in the data. This scatter is once again attributed to real variation in bird impacts. There do not appear to be any significant trends in the data. The oblique impact cases produce slightly lower values of rise time. However, the enormous scatter makes any firm conclusion questionable. The "squash-up" time appears to be a reasonable nondimensionalizing quantity for the rise time. Although the scatter in the data is great, a reasonable average value to use for the nondimensional rise time is 0.2.

2.4 SUMMARY

The experimental results displayed in Section 2.3 clearly show that the nondimensionalizing quantities derived in Section 2.2 are valid quantities with which to describe the forces generated by birds at impact. A generalized force-time bird impact profile is displayed in Figure 14. This generalized profile is consistent with the data and properly accounts for bird mass, bird size, impact velocity, and impact obliquity.

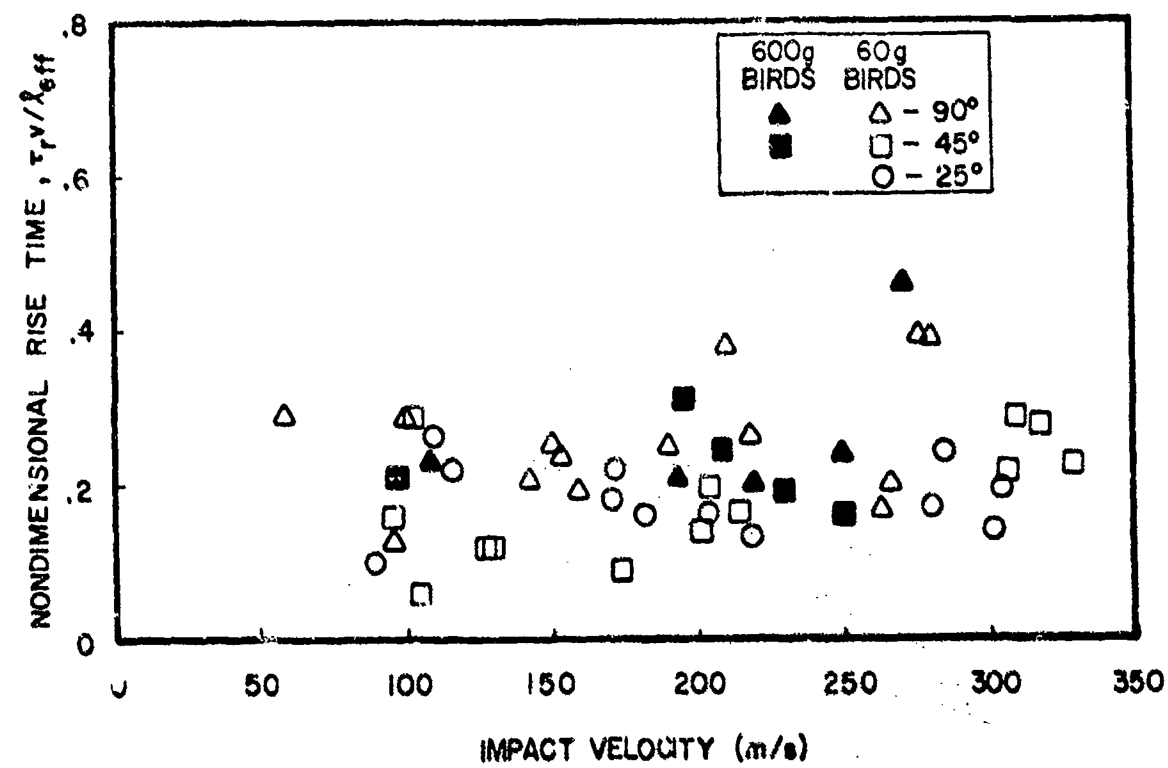

Figure 13. Nondimensional rise time versus impact velocity.

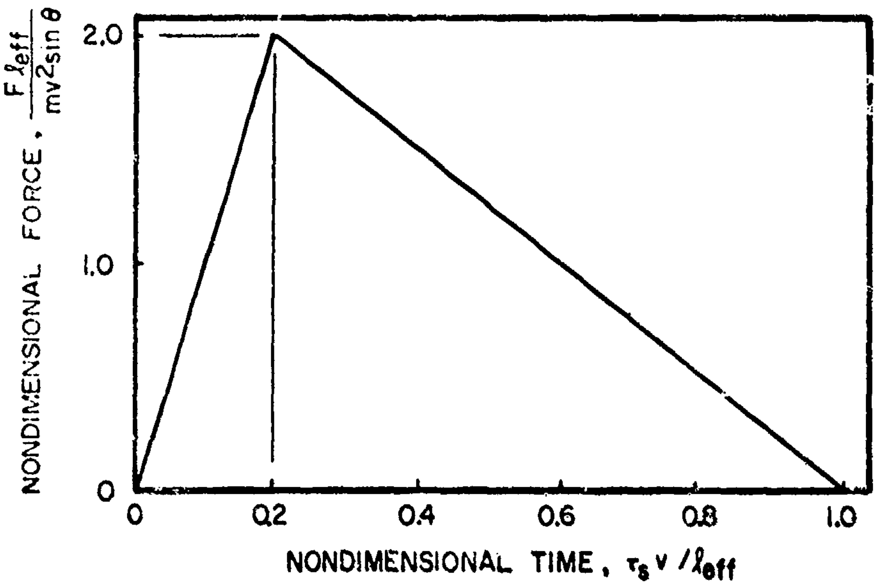

Figure 14. Generalized bird impact force-time profile.

SECTION III

BIRD IMPACT PRESSURES

To fully understand and analyze some aspects of windshield response to bird impact it is necessary to have more detailed knowledge of the impact loading process. In particular, the spatial distribution of the impact forces must be known. An experimental program was, therefore, undertaken to measure the spatial and temporal distribution of the pressures exerted on a rigid target during a bird impact. Pressure data was collected for a wide range of impact parameters. Bird masses ranging from 60 g to over 4 kg were employed. Velocities ranging from < 100 to ∿ 300 m/s were investigated. Impact obliquities of 90°, 45°, and 25° were studies. The data was collected, reduced, and analyzed, and is presented in this section.

3.1 EXPERIMENTAL TECHNIQUES

Most of the experimental work reported in this section was conducted at the AFML/UDRI facilities at Wright-Patterson Air Force Base. For bird sizes of over 1 kg the testing was conducted at Arnold Engineering Development Center (AEDC) in Tullahoma, Tennessee.

3.1.1 Bird Launching

The AFML/UDRI bird launching facility, described in Section 2.1, was also employed for the pressure testing. The launch technique, velocity, measurement, and bird observation techniques were identical to those used for the total force measurements.

The AEDC facility employs very similar techniques for launching birds. They used a compressed gas launch technique and place the birds in a balsa wood sabot. The sabot is stripped from the bird in a converging tube stripper. The AEDC facility is an outdoor facility. The most significantly different feature between the AEDC facility and the AFML/UDRI facility is the very long free flight of the bird from the sabot stripper muzzle to the target at AEDC. To prevent the birds from being unacceptably altered by the high aerodynamic forces during free flight, the birds are placed in light nylon bags. The long free flight of the bird also introduces uncontrollable pitch and yaw in bird orientation at the target. The presence of pitch and yaw at impact has proved extremely difficult to account for in data analysis. The effect of bagging the birds is unknown, but is assumed to have negligible effect on impact pressures. The AEDC facility is described in much greater detail in Reference 3.

3.1.2 Pressure Measurement

The measurement of impact pressures presents a number of difficulties. The impact shock pressures can be extremely high (several hundred MN/m^2). The pressure sensing device must be capable of measuring and withstanding these high pressures. The duration of the impact is relatively short (hundredths of μs) and there could be important transient pressure excursions. The pressure sensing and recording system must, therefore, have adequate bandwidth to detect and record important pressure transients.

A commercially available piezoelectric quartz pressure transducer was selected as the basic sensing device. These transducers employ a compact impedance converter physically located in the coaxial line close to the crystal. Since these transducers are not designed for impact testing, considerable experimentation and calibration was necessary to verify their operation. A calibration method for the transducers was developed to verify the applicability of the manufacturer's calibration data to the unidirectional axial loads anticipated[1]. A device was fabricated to enable the unidirectional axial loads similar to bird/plate impact loads to be applied to the transducer. Measurements were taken to determine the response of the transducers. It was concluded that the transducers provided reliable, accurate, pressure data over the range of pressures and frequencies expected. The transducers have a specified pressure range of 0 to 700 MN/m^2, and a specified bandwidth from 0 to 100 kHz. The transducers were mounted in a heavy steel plate. They were mounted such that the sensing surface of the transducers was flush with the surface of the plate. Birds were then impacted on the plate in such a manner that the transducers were directly struck by the bird. A photograph of the AFML/UDRI pressure plate is displayed in Figure 15. Up to eight transducers were mounted in this plate. The pressure signals were recorded on both oscilloscopes and an FM tape recorder.

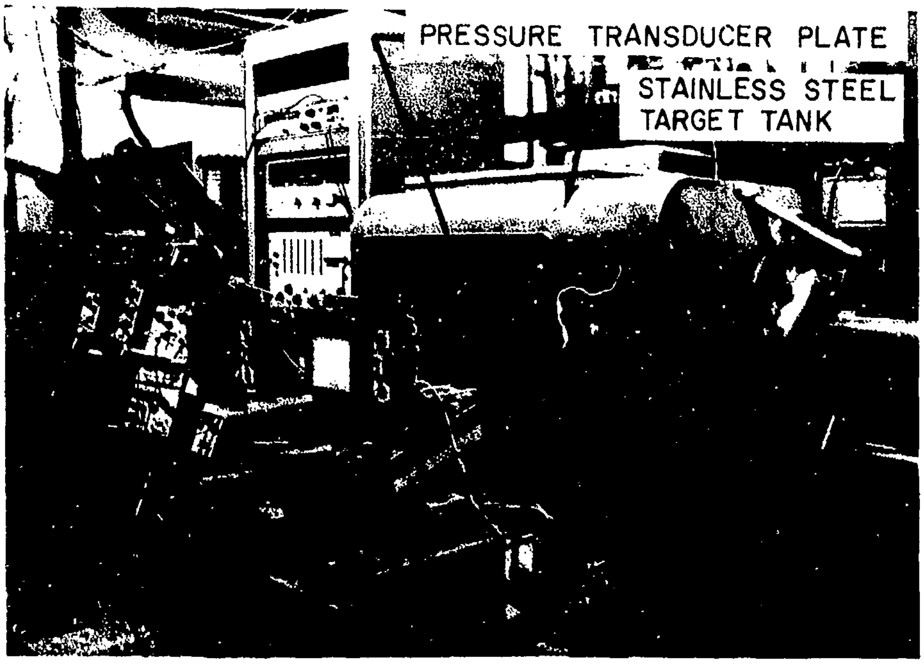

Figure 15. The AFML/UDRI pressure plate.

A photograph of the AEDC pressure plate and target area is displayed in Figure 16. This target plate was 76 cm square and 10 cm thick. Up to 29 pressure transducers could be mounted in the plate. The pressure signals were recorded on FM tape recorders.

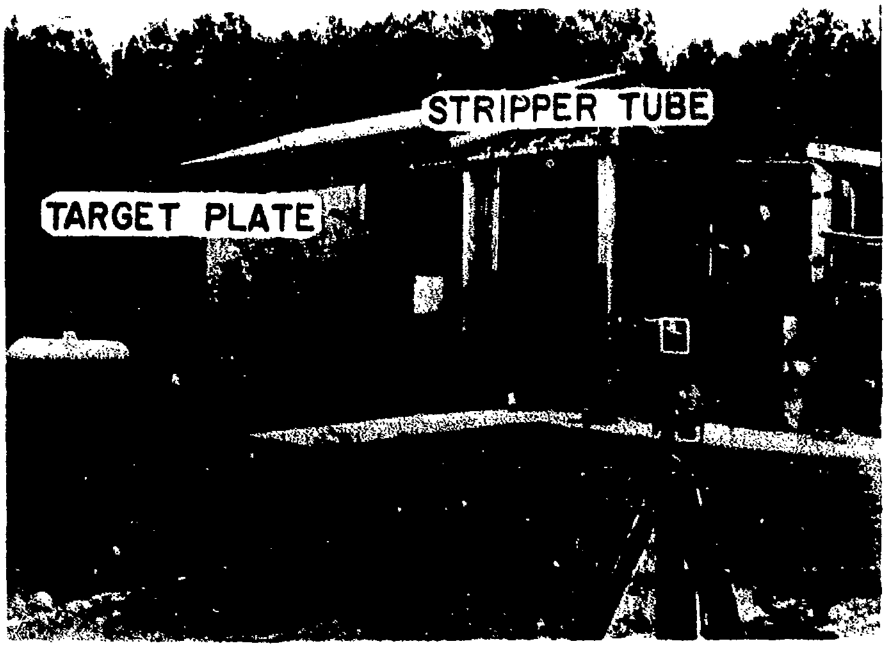

Figure 16. The AEDC pressure plate and target area.

The data from both facilities was collected at UDRI where it was reduced and analyzed. A typical pressure trace from the UDRI facility is displayed in Figure 17.

3.2 THEORETICAL CONSIDERATIONS

In order to facilitate reduction and analysis of the large body of data collected, a theoretical description of bird impact was undertaken. This analysis was not intended to provide a rigorous description of bird impact, but rather to provide theoretical guidance to the experiments and data reduction process. A parallel effort discussed in detail by Ito, et al.[4], treats in greater detail the more rigorous problem of analytical modeling.

To develop a theoretical description of the impacts, the physical phenomena which control the process must be identified or postulated. The impact of a bird on a rigid plate was assumed to be a nonsteady fluid dynamic process. The entire impact may then be divided into four phases. The first phase is the initial impact phase in which very high shock pressures are generated between the bird and the target. The release of this shocked material results in a decaying pressure. The pressure decays until the third phase of the impact is reached. During this phase the bird flows

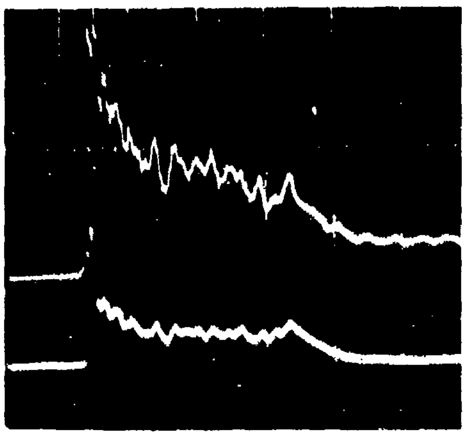

Shot No. 6049; Chicken mass 0.475 kg; Velocity 253 m/s; Horizontal scale 200 μs/cm; Upper trace 12.7 mm off-center with 15.1 $MN/m^2/cm$ vertical scale; Lower trace on center with 56.1 $MN/m^2/cm$ vertical scale.

Figure 17. A typical bird impact pressure record.

steadily onto the plate. This part of the process might be regarded as jet flow. The final phase of the impact occurs as the trailing end of the bird approaches the plate and the pressures once again fall to zero. These various phases are illustrated in Figure 18 and are described in some detail in the following paragraphs.

3.2.1 Initial Impact Phase

When a bird impacts a target plate, the particles at the front surface of the projectile (bird) are instantaneously brought to rest relative to the target face and a shock propagates into the bird as shown in Figure 18. As the shock wave propagates into the bird it brings the bird material behind the shock to rest. The pressure in the shock compressed region is initially very high and is uniform across the impact area. The edge of the projectile is a free surface and the material near the edge is subjected to a very high stress gradient. This stress gradient causes the material to accelerate radially outward and a release wave is formed. The arrival of this release wave at the center of the bird marks the end of the initial impact and the beginning of the decay process.

3.2.1.1 Normal Impact

For the normal impact of a cylinder on a rigid plate, the flow across a shock can be considered one-dimensional, adiabatic, and irreversible. The pressure behind the shock may then be derived from the shock relation as[5]

$$P = \rho v_s v \ , \tag{5}$$

where ρ is the density of the bird, v_s is the shock velocity, and v is the impact velocity. The shock pressure, therefore, depends not only on the impact velocity, but also on the shock velocity (which is, in general, a function of the impact velocity) and the bird density.

The density of both small birds (60 g) and medium birds (600 g) was measured. The birds were accurately weighed, then immersed in water to determine the displaced volume. Detergent was added to the water to facilitate total wetting of the bird and elimination of bubbles trapped in the feathers. The density of the birds (chickens) was found to be 0.95 ± 0.02 g/cm^3. There was no significant difference between the density of the 60 g birds and the density of the 600 g birds.

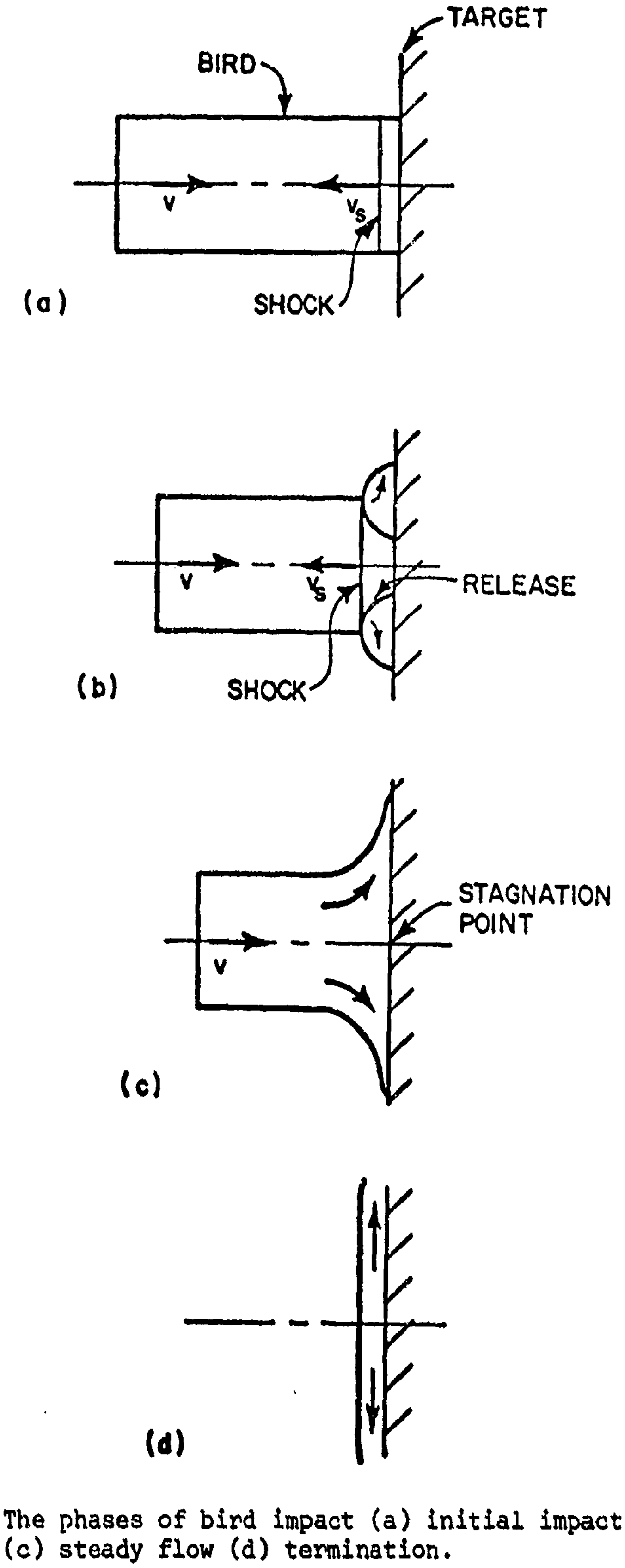

Figure 18. The phases of bird impact (a) initial impact (b) impact decay (c) steady flow (d) termination.

As the principal constituent of flesh is water, it was assumed that the lower average of birds is due to the presence of porosity. A good material model was found to be gelatin with an initial density of 1.05 g/cm^3 and an air filled porosity of 10 percent (net density of 0.95 g/cm^3)[6]. For this material, Wilbeck[6] using mixture theory, calculated the shock velocity and impact (or Hugoniot) pressure as a function of impact velocity. The results, for normal impact, are shown in Figure 19. The pressures are extremely high (100-500 MN/m^2) over the range of impact velocities of interest.

3.2.1.2 Oblique Impact

For the oblique impact of a projectile on a rigid plate, a coordinate transformation aids in the understanding of the shock process. Figure 20 shows a cylinder with an initial velocity, v, impacting a stationary plate at angle, Θ. The component of projectile velocity normal to the plate is v sin Θ and the component tangential to the plate is v cos Θ. The initial shock pressure is related only to the component of velocity normal to the surface and is given by a transformed Equation (5) as

$$P = \rho v_s^* v (\sin \Theta) , \qquad (6)$$

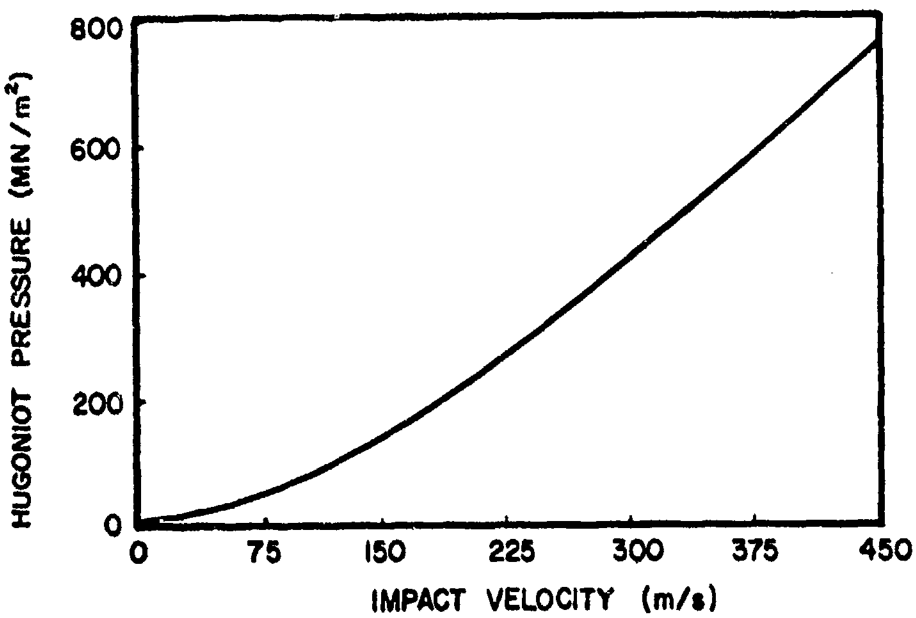

Figure 19. The shock pressure for birds[6] (gelatin with 10 percent porosity.)

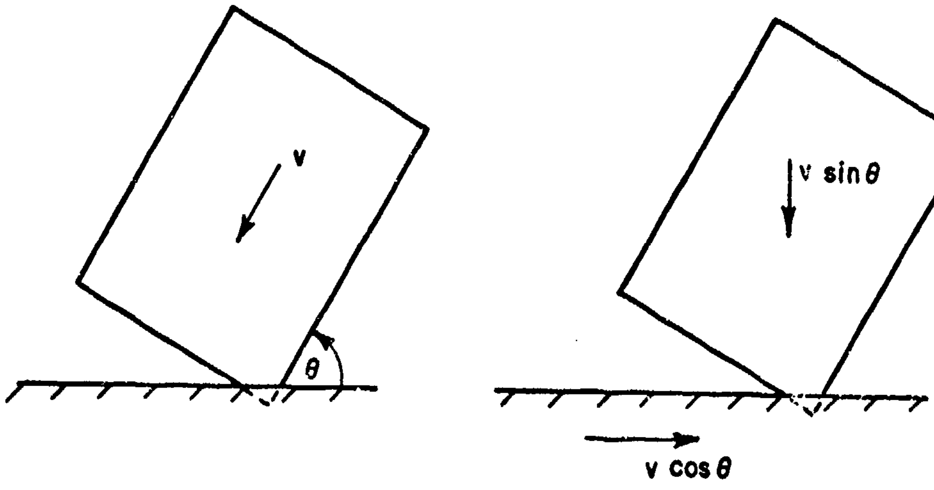

Figure 20. An oblique impact.

where v_s^* is the shock velocity corresponding to an impact velocity of v sin Θ. Because the shock velocity is a relatively strong function of the impact (normal) velocity, the shock pressure does not vary exactly as sin Θ. The shock pressures for gelatin with 10 percent porosity at 45° and 25° were determined by Wilbeck[6] and are shown in Figure 21.

3.2.2 Impact Pressure Decay

At initial impact a shock begins to propagate into the projectile and radial release waves propagate in towards the center from the free surface edges of the bird as shown in Figure 18 (b). The problem can no longer be considered to be one-dimensional in nature. For the normal impact of a cylinder, the problem is two-dimensional and axi-symmetric.

Figure 22 shows the release regime for impact of a cylinder with an original length to diameter ratio of 2. Figure 22 (b) illustrates the projectile just after impact. The pressure at point B is given by Equation (5). Figure 22 (c) shows when the release waves have converged at point B, the center of impact. The pressure on the target at the center of impact now begins to decay. Figure 22 (d) shows when the release waves have converged at the center of the shock, and a region of fully shocked material no longer exists. The curvature of the shock is due to the release process, which has weakened the shock more at the edges than at the center.

The duration of the full shock pressure, Equation (5), at the center of impact is given by the time that it takes the initial release

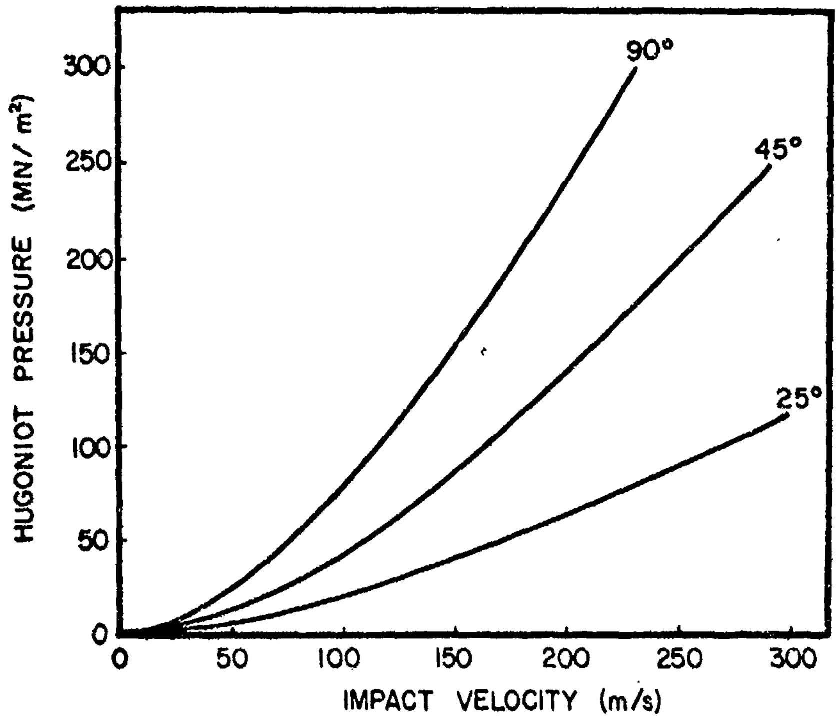

Figure 21. The variation of bird impact pressure with impact angle. (Gelatin with 10 percent porosity).

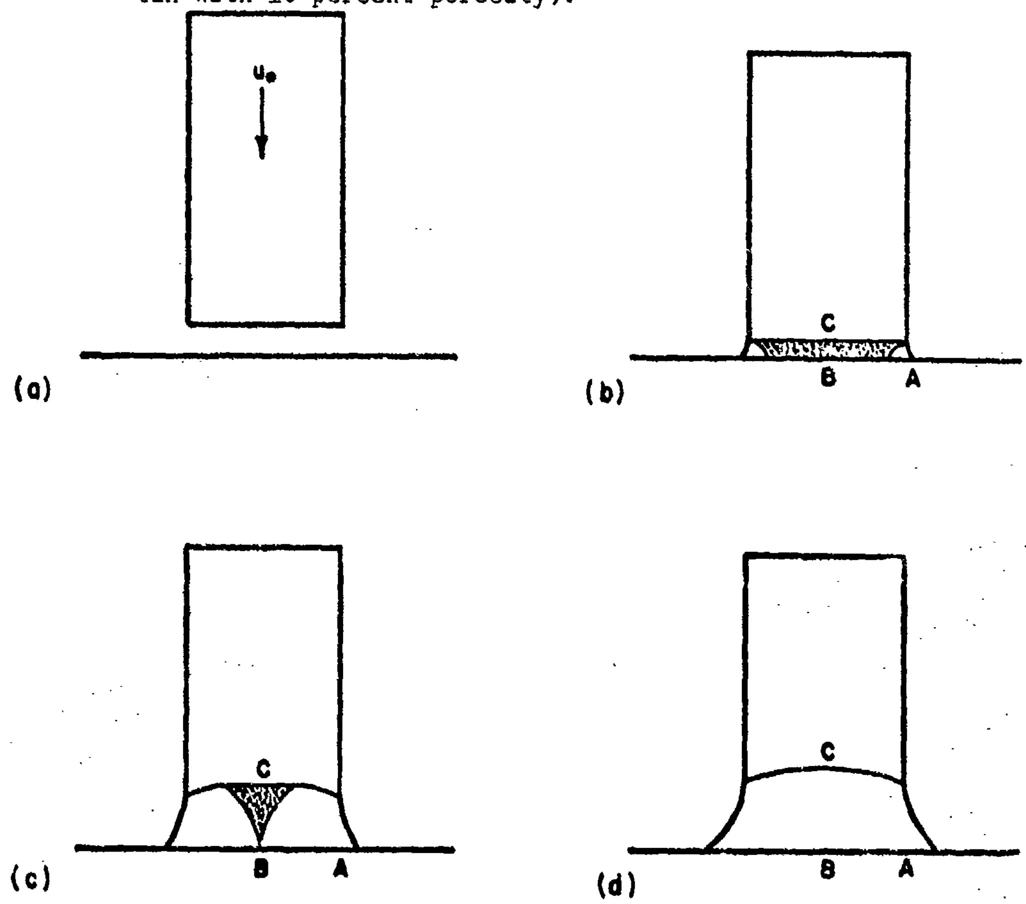

Figure 22. Shock and release in a bird impact.

wave to reach the center. The release wave is a fan of weak expansion waves and can be considered isentropic. Thus, the velocity of the initial release wave is equal to the speed of sound in the shocked material, c_r. The expression for the time necessary for the release wave to reach the center of impact is

$$t_r = a/c_r, \quad (7)$$

where a is the initial radius of the cylinder. Wilbeck[6] has calculated c_r for gelatin with 10 percent porosity as a function of the impact velocity. Using these values he calculated the initial release time using Equation (7). Figure 23 shows the relationship between t_r and the impact velocity, v, for cylindrical projectiles of various radii.

Another important time is the time at which the release wave front converges at the center of the shock wave. Since the wave speed in the fully shocked medium is always greater than the shock speed, the release wave will interact with progressively more of the shock as the impact continues. Figure 22 (d) shows the condition in which the release wave front has just converged on point C, the center of the shock. After this time, the pressure in the region behind the shock will rapidly decay and the

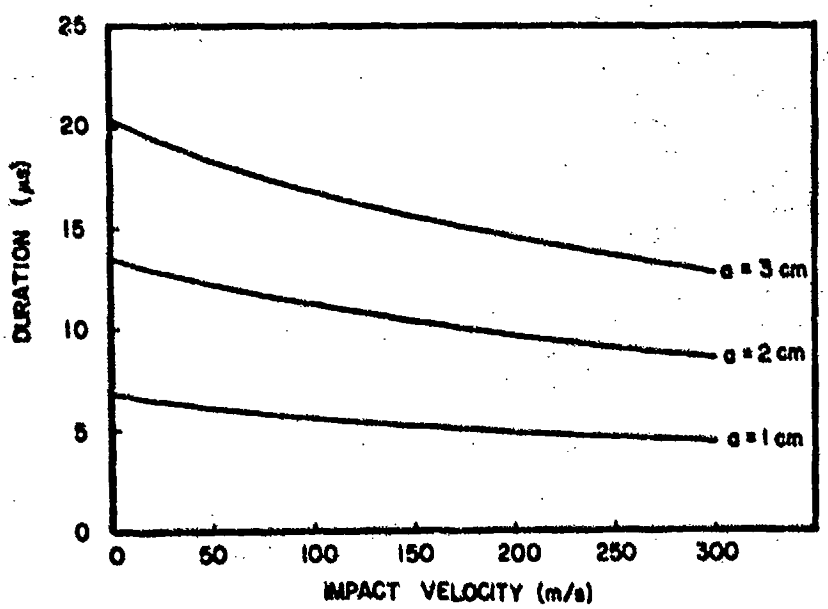

Figure 23. Shock release time versus impact velocity for birds (gelatin with 10 percent porosity).

shock will be weakened. This time, t_c, may be derived from geometric considerations. In order for the release wave starting at point A to intersect the shock at point C, it must travel a radial distance, a, and an axial distance equal to the axial distance traveled by the shock. At the time of intersection, the shock has propagated a distance

$$x_s = (v_s - v)\, t_c \quad ,$$

where $(v_s - v)$ is the velocity of the shock relative to the target. Therefore, the release waves have traveled a distance

$$x_r = (x_s^2 + a^2)^{1/2}.$$

The release wave travel time, t_c, is given by

$$t_c = x_r/c_r.$$

By substituting and rearranging we obtain

$$t_c = \frac{a}{(c_r^2 - (v_s - v)^2)^{1/2}} \; . \qquad (8)$$

From Equation (8) an expression can be derived for the critical projectile length, ℓ_c, which is the length for which the radial release wave will just intersect the shock axis, (point C), as the shock reaches the end of the projectile

$$\ell_c = v_s t_c \; . \qquad (9)$$

Combining Equations (8) and (9) and nondimensionalizing to the bird diameter we obtain

$$(\ell/d)_c = \frac{v_s}{2\,(c_r - (v_s - v)^2)}\, 1/2 \, . \qquad (10)$$

For a projectile with an $\ell/d > (\ell/d)_c$, the shock will be severely weakened by the release waves prior to reaching the projectile end and the reflection will be greatly reduced or eliminated.

Wilbeck[6] calculated $(\ell/d)_c$ for gelatin with 10 percent porosity and Figure 24 shows a plot of the results. For a projectile of sufficient length, steady flow should be set up after several reflections of the radial release waves. A projectile with a length somewhat greater than ℓ_c should undergo complete shock decay to steady flow. As birds have an ℓ/d of about 2 to 3, a steady flow region is expected to exist. A longer steady flow regime is expected at low velocities than at high velocities.

The details of pressure variation with time during the decay process are extremely difficult to predict. In addition to the geometrical complexities, complete shock release material properties for the bird must be known. These are not currently available and would probably be difficult to obtain. Finite difference modelling of the process as reported by Ito, et al.[4] is the most promising overall approach to properly modelling the decay process.

Oblique impact effects further complicate the details of the release process. However, the decay times, as calculated for normal impacts, will be nearly the same.

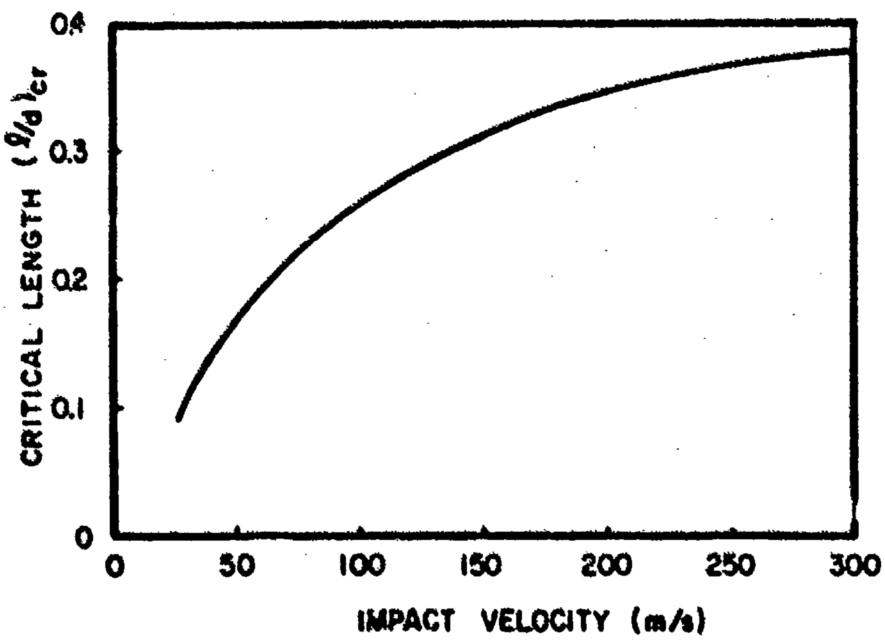

Figure 24. Variation of critical length with impact velocity for birds (Gelatin with 10 percent porosity).

3.2.3 Steady Flow

As the radial pressures decrease during the shock pressure decay, shear stresses develop in the projectile material. If the shear strength of the material is sufficient to withstand these shear stresses, the radial motion of the projectile will be restricted. If, however, the shear stresses in the projectile are greater than the shear strength of the material, the material will "flow". The shear strength of birds is so low that the pressures generated are usually sufficient to cause flow. The bird can be considered to behave as a fluid. After several reflections of the release waves, a condition of steady flow is established and steady pressure and velocity fields are established.

3.2.3.1 Normal Impact

During the release phase, the shock ... weakened by the release waves. For a subsonic impact, the shock wave will be ultimately eliminated by the release. In a supersonic impact the shock wave will not disappear. The shock propagation velocity will decrease until it becomes equal to the impact velocity (a standing shock). Behind this standing shock, the flow will be subsonic and will follow steady flow streamlines. The velocity and pressure fields in the fluid will be quite different for the two cases. The presence of porosity in birds results in a very low sonic velocity (40 m/s for gelatin with 10 percent porosity). Bird impacts are, therefore, most probably supersonic.

Using potential flow theory, Wilbeck[6] calculated the steady flow pressure for a supersonic bird impact at normal incidence. The results are displayed in Figure 25. He found that the pressure at the center of impact (the stagnation pressure) could be approximately given by the expression

$$P_s \approx \frac{1}{2} \rho_o v^2 , \qquad (11)$$

where ρ_o is the density of the material with zero porosity. This implies that the steady flow pressure at the center of impact is almost independent of porosity. The decrease in density due to porosity is apparently offset by the increase in compressibility.

Wilbeck[6] also calculated the radial distribution of pressure for a normal supersonic impact. The results for gelatin with 10 percent

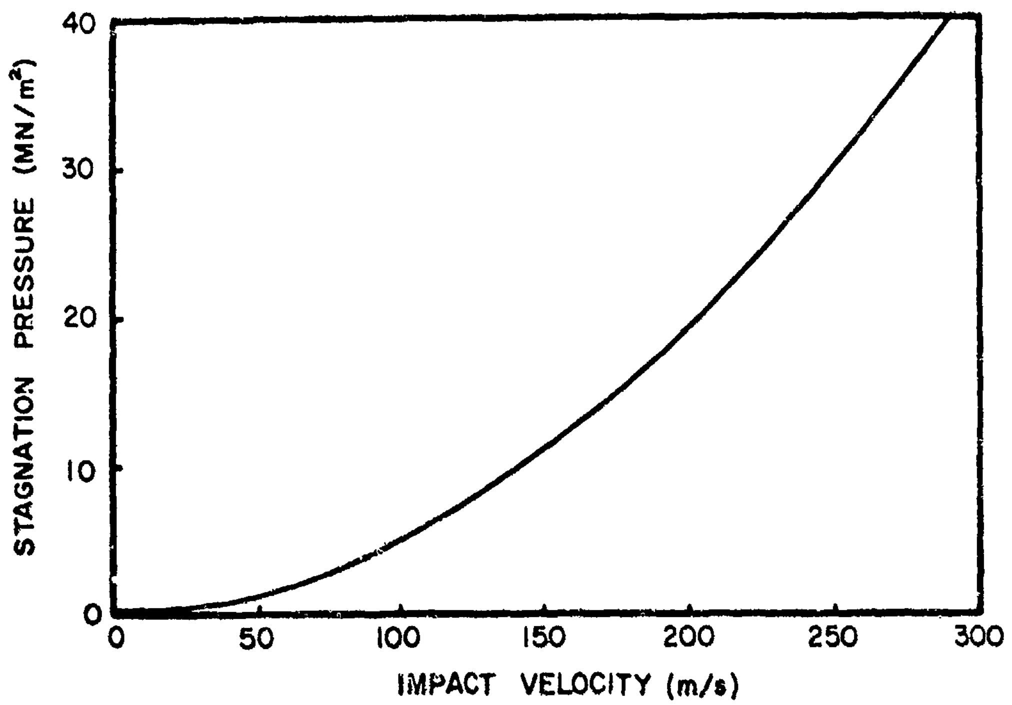

Figure 25. Steady state velocity.

are shown in Figure 26. The pressure is nondimensionalized by dividing by the steady flow pressure for an incompressible fluid, $\frac{1}{2}\rho v^2$, and the radial distance from the center, r, is nondimensionalized by dividing by the radius of the projectile, a.

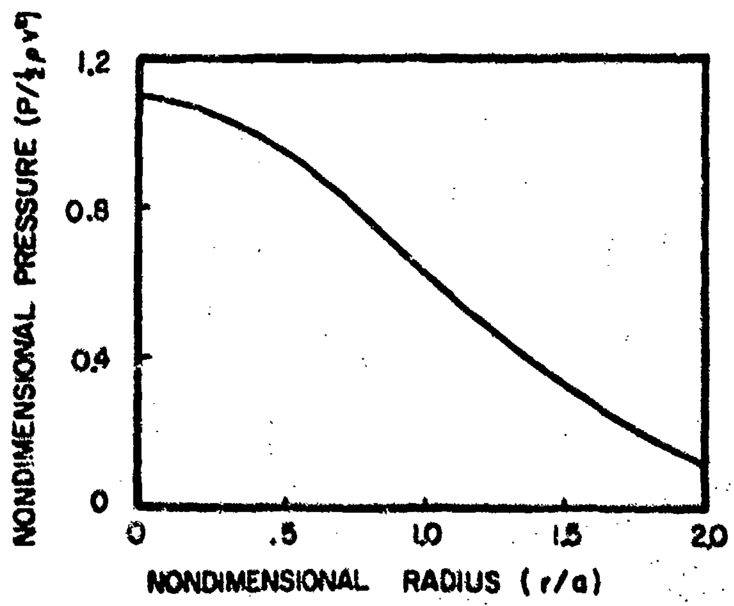

Figure 26. Normal impact pressure distribution for birds (Gelatin with 10 percent porosity).

The equation which describes this distribution is

$$P/P_s = \exp\left(-\beta(r/a)^2\right) , \qquad (12)$$

where P_s is the stagnation pressure and $\beta = 2P_s/\rho v^2$. From Equation (11) it is apparent that $\beta \sim \rho_o/\rho$ where $\rho_o = 1.05$ g/cm^3.

3.2.3.2 Oblique Impact

Figure 27 shows the steady flow of an oblique impact of a cylinder of fluid on a rigid plate. From momentum considerations it can be seen that the majority of fluid will flow "downstream" on the obtuse side of the impact. The stagnation point shifts "upstream" to the acute side of the center of impact. As long as a stagnation point exists, the full stagnation pressure will occur as given by Equation (11). The maximum pressure generated during steady flow will, therefore, be independent of the angle of impact. However, the distribution of pressure over the surface will be greatly dependent on the impact angle.

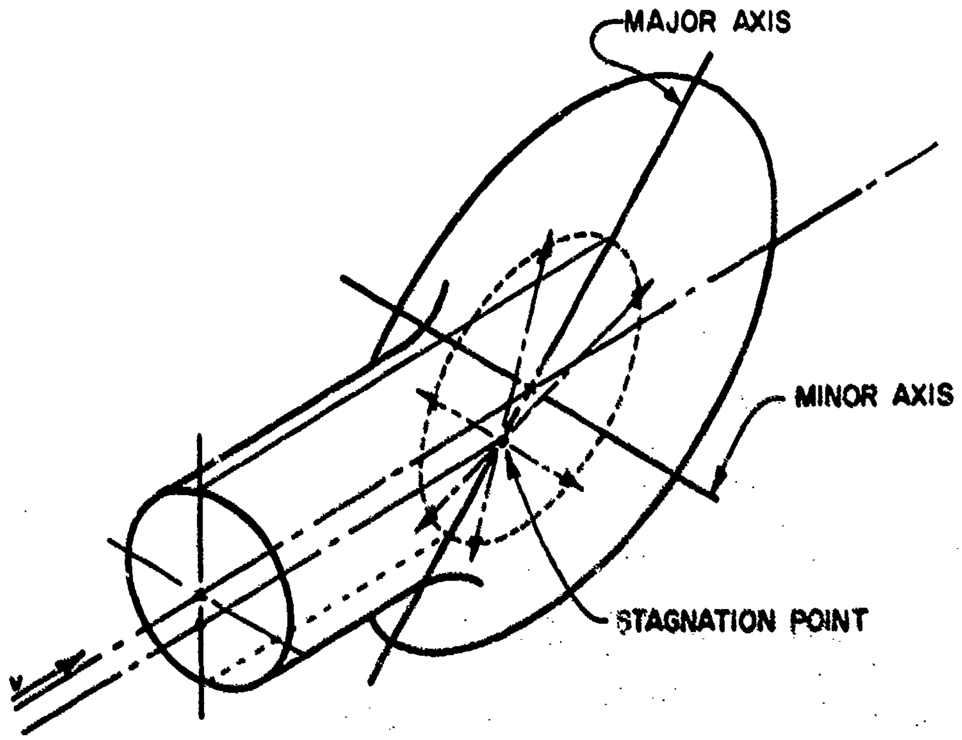

Figure 27. Oblique impact.

The distribution of pressure in an oblique cylindrical impact is difficult to analyze as it is a three-dimensional fluid dynamic problem. A number of authors have treated the two-dimensional case of the oblique impact of a sheet[7,8,9]. Taylor[10] also did some experimental investigations of flow in an oblique cylindrical jet. However, no satisfactory description of oblique jet pressures was found in the literature. Thus, an analytic investigation of oblique jet flow was undertaken as a part of this program.

Three-dimensional potential flow theory was used to develop a model for predicting the pressure distribution produced by the steady flow of a cylindrical jet impacting on a flat plate. It was assumed that the pressure distribution, as calculated for this fluid dynamic problem, would provide a reasonable description of the steady flow portion of a bird impact. Assumptions were made that the flow could be treated as incompressible and irrotational. These assumptions are supported by the fact that (1) the steady state pressures measured in the experiments are small in comparison to the pressures required to produce significant density changes in water and, (2) the time over which the steady flow exists is small in comparison to the time required to establish strong vorticity in the flow. It should be noted that the steady flow portion of a bird impact is ideally suited for modelling by potential flow theory because there is no entrainment of surrounding fluid.

The model was based on superposition of two elementary solutions to the Laplace equation

$$\Delta^2\phi = \frac{\partial^2\phi}{\partial x^2} + \frac{\partial^2\phi}{\partial y^2} + \frac{\partial^2\phi}{\partial z^2} ,$$

which is the governing equation for steady, incompressible, irrotational flow. The two elementary solutions used were; (1) the uniform flow of a fluid in a round duct and, (2) the uniform distribution of planar sources over an elliptical area. The coordinate system used to model the flow is shown in Figure 28. Let $(0, \eta, \zeta)$ represent the coordinates of the location of a point source in the y-z plane. The velocity components induced by this source are given by[11]

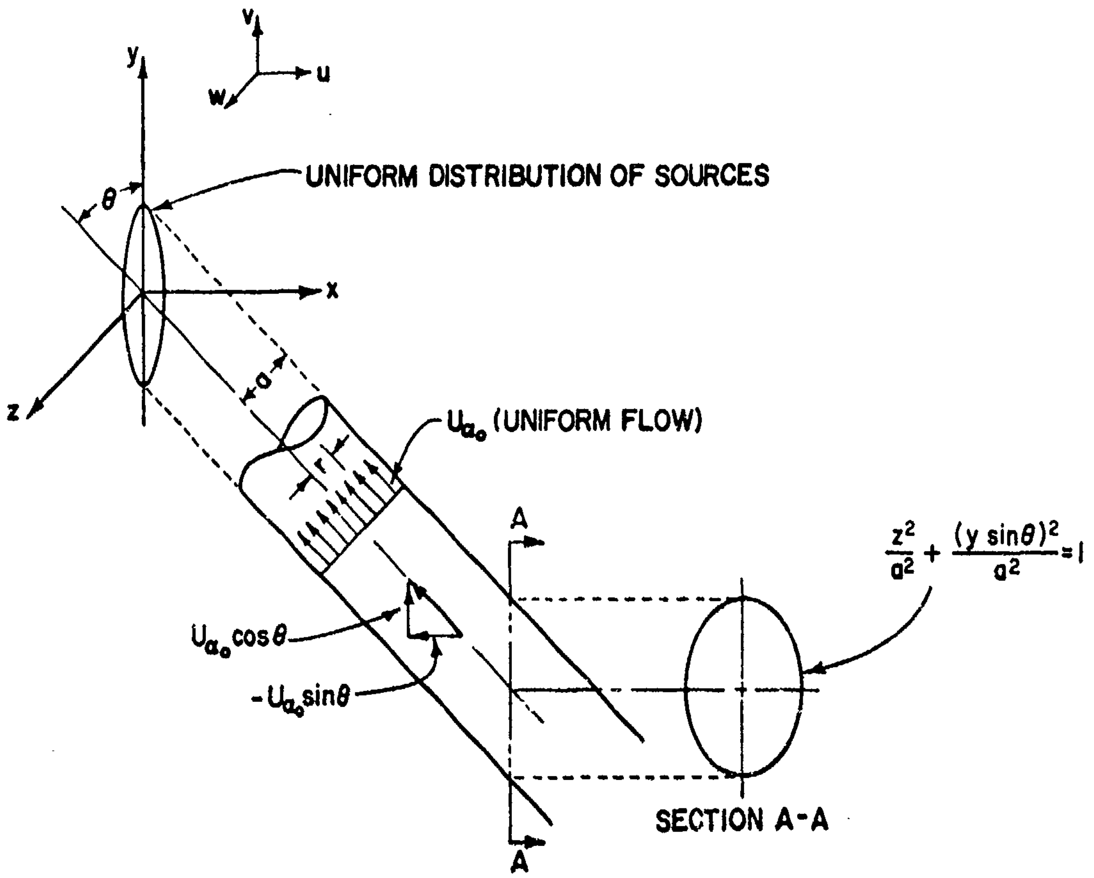

Figure 28. Oblique impact potential flow model.

$$u = \frac{q}{4\pi} \frac{x}{[x^2 + (y-\eta)^2 + (z-\zeta)^2]^{3/2}} ,$$

$$v = \frac{q}{4\pi} \frac{(y-\eta)}{[x^2 + (y-\eta)^2 + (z-\zeta)^2]^{3/2}} ,$$

$$w = \frac{q}{4\pi} \frac{(x-\zeta)}{[x^2 + (y-\eta)^2 + (z-\zeta)^2]^{3/2}} ,$$

where q is the strength of the source. The velocity field induced by a uniform surface distribution of sources in the y-z plane of strength q" per unit area is given by[12]

$$u\ (x,y,z) = \frac{q''}{4\pi}\, x \int_{\zeta_1}^{\zeta_2}\int_{\eta_1}^{\eta_2} \frac{d\eta d\zeta}{[x^2 + (y-\eta)^2 + (z-\zeta)^2]^{3/2}} ,$$

$$v\ (x,y,z) = \frac{q''}{4\pi} \int_{\zeta_1}^{\zeta_2}\int_{\eta_1}^{\eta_2} \frac{(y-\eta)\ d\eta d\zeta}{[x^2 + (y-\eta)^2 + (z-\zeta)^2]^{3/2}} , \qquad (17)$$

$$w\ (x,y,z) = \frac{q''}{4\pi} \int_{\zeta_1}^{\zeta_2}\int_{\eta_1}^{\eta_2} \frac{(z-\zeta)\ d\eta d\zeta}{[x^2 + (y-\eta)^2 + (z-\zeta)^2]^{3/2}} .$$

Integration of the above three equations over the elliptical area bounded by

$$\frac{\zeta^2}{a^2} + \left(\frac{y \sin \Theta}{a}\right)^2 = 1$$

(the projection of the jet on the plane) cannot be carried out in closed form. They can be integrated over rectangular areas, however. Therefore, the procedure used was to approximate the elliptical source area by square sources and then sum the solutions of all the squares. The velocity field induced by the uniform distribution of sources over a rectangular element whose corners are located at (η_1, ζ_1), (η_1, ζ_2), (η_2, ζ_2), and (η_2, ζ_1) in the y-z plane is given by the following expressions (page 12 of Reference 12);

$$u\ (x,y,z) = \frac{q''}{4\pi}\left[\tan^{-1}\frac{(z-\zeta_2)\ (y-\eta_2)}{xr_3} + \tan^{-1}\frac{(z-\zeta_1)\ (y-\eta_1)}{xr_1} - \tan^{-1}\frac{(z-\zeta_1)\ (y-\eta_2)}{xr_2} - \tan^{-1}\frac{(z-\zeta_2)\ (y-\eta_1)}{xr_4}\right],$$

$$v(x,y,z) = \frac{q''}{4\pi} \ln\left\{\frac{[r_3 + (\zeta_2 - z)]}{[r_4 + (\zeta_2 - z)]} \frac{[r_1 + (\zeta_1 - z)]}{[r_2 + (\zeta_1 - z)]}\right\},$$

$$w(x,y,z) = \frac{q''}{4\pi} \ln\left\{\frac{[r_3 + (\eta_2 - y)]}{[r_2 + (\eta_2 - y)]} \frac{[r_1 + (\eta_1 - y)]}{[r_4 + (\eta_1 - y)]}\right\},$$

where $r_1 = \sqrt{x^2 + (y-\eta_1)^2 + (z-\zeta_1)^2}$, $r_2 = \sqrt{x^2 + (y-\eta_2)^2 + (z-\zeta_1)^2}$

$r_3 = \sqrt{x^2 + (y-\eta_2)^2 + (z-\zeta_2)^2}$ and $r_4 = \sqrt{x^2 + (y-\eta_1)^2 + (z-\zeta_2)^2}$.

These equations exhibit a characteristic which permits a relatively simple approach to the solution as follows;

$u(0,y,z) = \frac{q''}{2}$ for any point on the rectangular surface area

and

$u(0,y,z) = 0$ for any point not on the rectangular surface area.

In order that the y-z plane represent a surface across which no mass flows, that is, a flat plate, the round jet flow and the flow due to the sources on all the square elements (whose sum approximates the elliptical area) must be superimposed such that u is zero on y-z plane. This condition is satisfied by setting the strength of the surface distribution, q", over each square element equal to

$$q'' = 2\, U_\infty \sin\Theta .$$

With the surface source strength per unit area so chosen, the U-component of velocity is identically zero over the entire y-z plane at x = 0. The V-component of velocity of the superimposed flow in the y-z plane at x = 0 over the elliptical area is given by

$$V(0,y,z) = U_\infty \cos\Theta + \frac{V_\infty \sin\Theta}{2\pi} \sum_k v_k(0,y,z) ,$$

where the summation is taken over each of the square areas comprising the elliptical area. The W-component of velocity of the superimposed flow in the y-z plane at x = 0 is given by

$$W\ (0,y,z) = \frac{U_\infty \sin \Theta}{2\pi} \sum_k w_k\ (0,y,z)\ .$$

The pressure on the plate over the elliptical area is then given by Bernoulli's equation,

$$p\ (0,y,z) = p\ \ + \frac{1}{2}\,\zeta_\infty\ \{[V\ (0,y,z)]^2 + [W\ (0,y,z)]^2\}.$$

Since p_∞ is atmospheric pressure, Bernoulli's equation can be written in terms of a pressure coefficient (equivalent to the nondimensionalized pressure) c_p, as

$$c_p = \frac{p-p_\infty}{\frac{1}{2}\zeta U_\infty^{\ 2}} = \frac{1}{U_\infty^{\ 2}} \left\{V^2 + W^2\right\} . \qquad (17)$$

A computer program was written to calculate the pressure coefficient. A listing is contained in Appendix A. Figure 29 shows the variation of the pressure coefficient calculated along the major axis of the elliptical impact area and plotted as a function of r, the projection of y in the y-z plane at x = 0 onto a plane perpendicular to the axis of the jet, (i.e. r = y sin Θ). The pressure coefficient at any point on the surface can be readily calculated. Since the model does not contain the vorticity which undoubtedly occurs, it does not reliably predict coefficients near the boundary of the jet (y = a/sin Θ). However, over the central portion of the jet the predictions should be reasonably accurate.

3.2.4 Flow Termination

During impact, bird material is "turned" near the target surface. As the fluid nears the target surface the velocity decreases and the local pressure increases. During steady flow a pressure field is set up in the

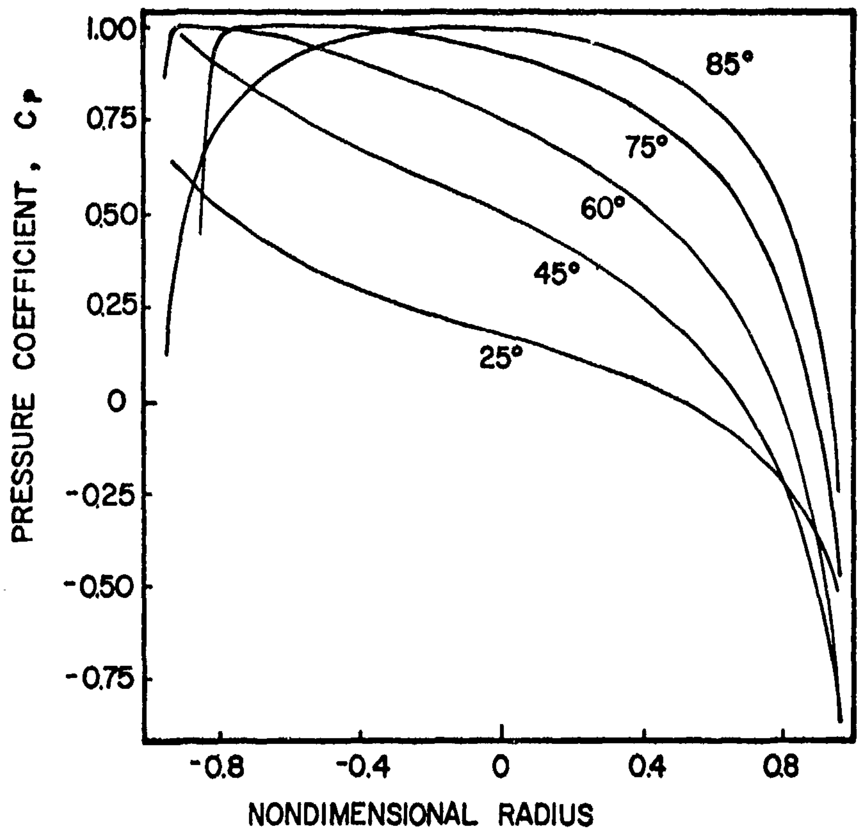

Figure 29. Pressure coefficient ($2P/\rho v^2$) versus nondimensional radius along the major axis of the impact for oblique impacts.

fluid. As the end of the projectile enters this pressure field, the field is disrupted due to the intrusion of a free surface (the end of the bird). Steady flow no longer exists and the pressures at the impact surface decrease. The pressure decrease continues until the end of the projectile reaches the surface of the plate. At this time the impact event is ended. The total duration of the impact is given by the expression $\tau = \ell/v_o$ as was found in Section II for impact forces.

3.3 EXPERIMENTAL RESULTS

Over sixty bird impact pressure data shots with 60 g birds and over fifty shots with 600 g birds were obtained at the AFML/UDRI facility. Normal (90°), 45°, and 25° impacts were obtained. Over seventy impacts were made with birds on the pressure plate at the AEDC facility. These birds ranged in mass from approximately 1 kg to approximately 4 kg. Of these latter shots, approximately ten provided useful quantitative information. A lack of control over bird orientation at impact precluded meaningful interpretation of the remaining data shots.

All the data was collected together at the AFML/UDRI facility where it was reduced and analyzed. Measurements of peak pressure, steady flow pressure, and pulse duration were obtained from the records. The results of these measurements, together with comparisons to the theoretical results derived in Section 3.2, are presented in the following sections.

3.3.1 Initial Impact Pressures

In Section 3.2.1 it was pointed out that the highest pressures generated during the impact should occur during the initial stages of the impact. The pressure should rise to the impact, or Hugoniot, pressure. This pressure was calculated by Wilbeck[6] using a bird model consisting of gelatin with 10 percent porosity and is shown in Figure 30. The initial impact pressures agree very well with the calculated pressure for large birds (i.e., 4 kg). However, the results for small birds show significant departures from prediction. The discrepancy appears to increase with decreasing bird size.

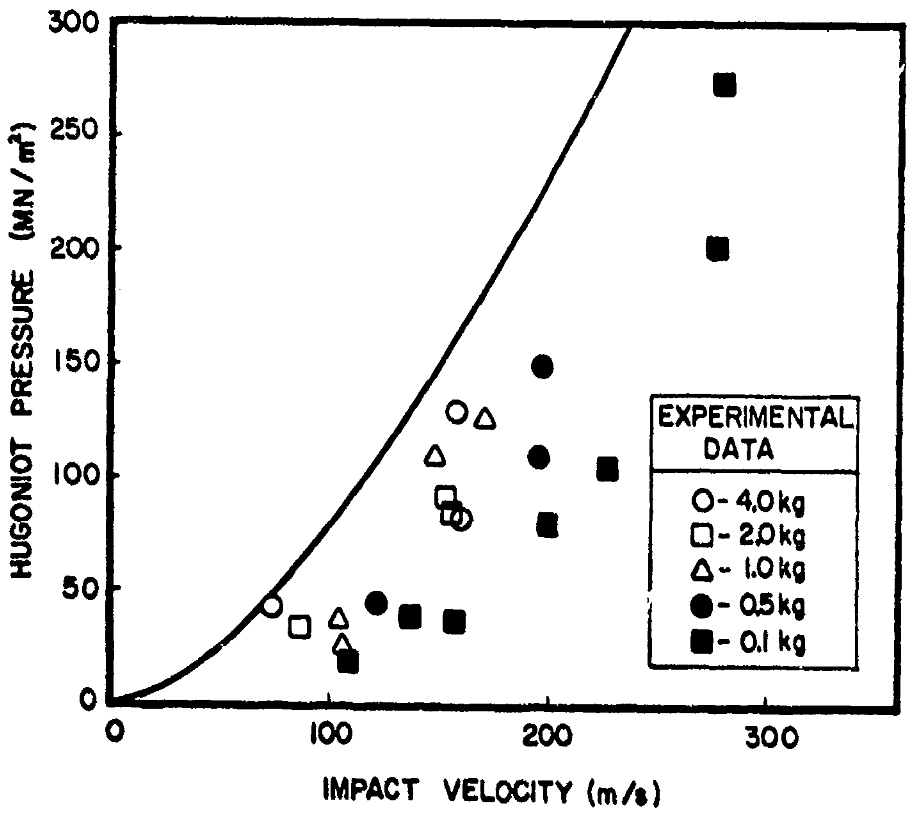

Figure 30. Initial impact (Hugoniot) pressures versus impact velocity for normal impact.

As pointed out in Section 3.2.1, the duration of the shock pressure is directly proportional to the bird diameter or radius. Therefore, larger birds produce high pressures for longer duration than do small birds. The limited bandwidth of the transducers (100 kHz) results in a significant attenuation of the measured signal for the short pulse durations which might be expected for small birds. It is, therefore, not entirely surprising that the full shock pressure is not detected in small bird impacts. However, the full shock pressure almost certainly occurs, although the duration is extremely short.

For oblique impacts, the shock pressure expected is that which corresponds to the normal component of impact velocity. The experimentally measured results and theoretical predictions are shown in Figure 31. Again, the results for large birds show good agreement with the prediction. The duration of the impact pressure was so short for small birds that reliable measurements of peak pressure could not be made. It is notable that at very low angles the impact pressure approaches the steady flow pressure and no impact spike would be expected. For 25° impacts, the impact pressure spike was much less pronounced than for 90° impacts. No reliable measurements of impact pressure were obtained at 25°.

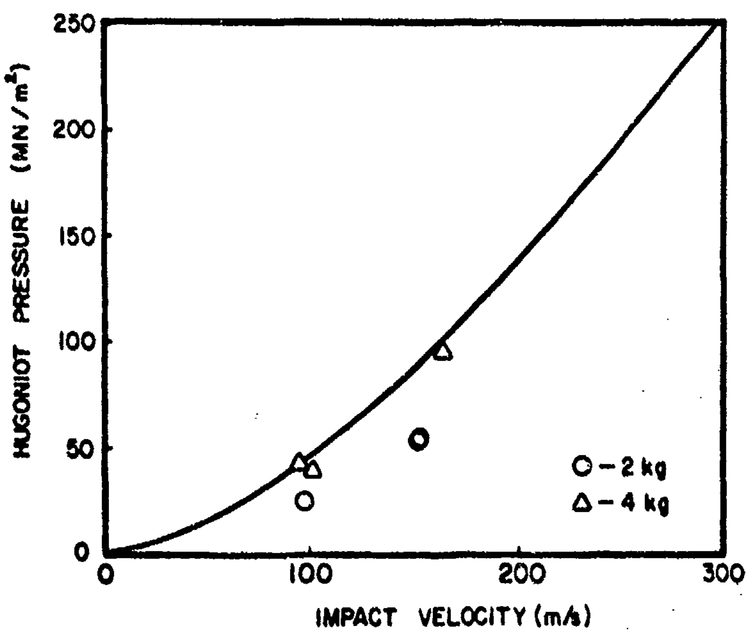

Figure 31. Initial impact (Hugoniot) pressures versus impact velocity for 45° impacts.

3.3.2 Impact Pressure Decay

As was pointed out in Section 3.2.2, it is not possible to calculate the details of the decay process unless the shock release properties of the bird material are known. As those properties are not known, the decay process cannot be calculated. However, the time taken for the release waves to completely overtake the shock front can be calculated. From these considerations, a critical length was found. For birds shorter than this critical length the shock pressure decay process never reaches steady flow value. For birds longer than this critical length steady flow must be established. Therefore, the critical length provides at least a first order approximation of the time at which the decaying shock pressures should reach the steady flow values. As several reflections of the release wave are probably required to establish steady flow, a precise value for this time cannot be determined. For birds striking end-on (that is the axis of the bird is parallel to trajectory) the length to diameter ratio varies from approximately two to approximately three. The results of Section 3.2.2 indicate that this should permit establishment of the steady flow process. Observation of a large number of bird impact pressure records indicate that for normal impact steady flow is generally established within half the impact duration.

For side-on impacts, the effective length to diameter ratio of a bird is about 0.3 to 0.4. This is less than the critical bird length derived in Section 3.2.2, and steady flow would not be expected to occur. A number of impacts at the AEDC facility were determined to have struck side-on. For these cases no steady pressure region was observed in the pressure records.

3.3.3 Steady Flow Pressures

For virtually all the impacts conducted on the pressure plate at the AFML/UDRI facility, a steady pressure region in the pressure record could be identified. In only three normal impact shots at AEDC was the orientation of the bird sufficiently axial that steady state pressures were established during impact. The center of impact data for normal impacts was collected and compared to the stagnation pressures as calculated in Section 3.2.3. The results are shown in Figure 32. The center of impact pressures are extremely close to the predicted stagnation pressure. There does not appear to be any significant difference between the small

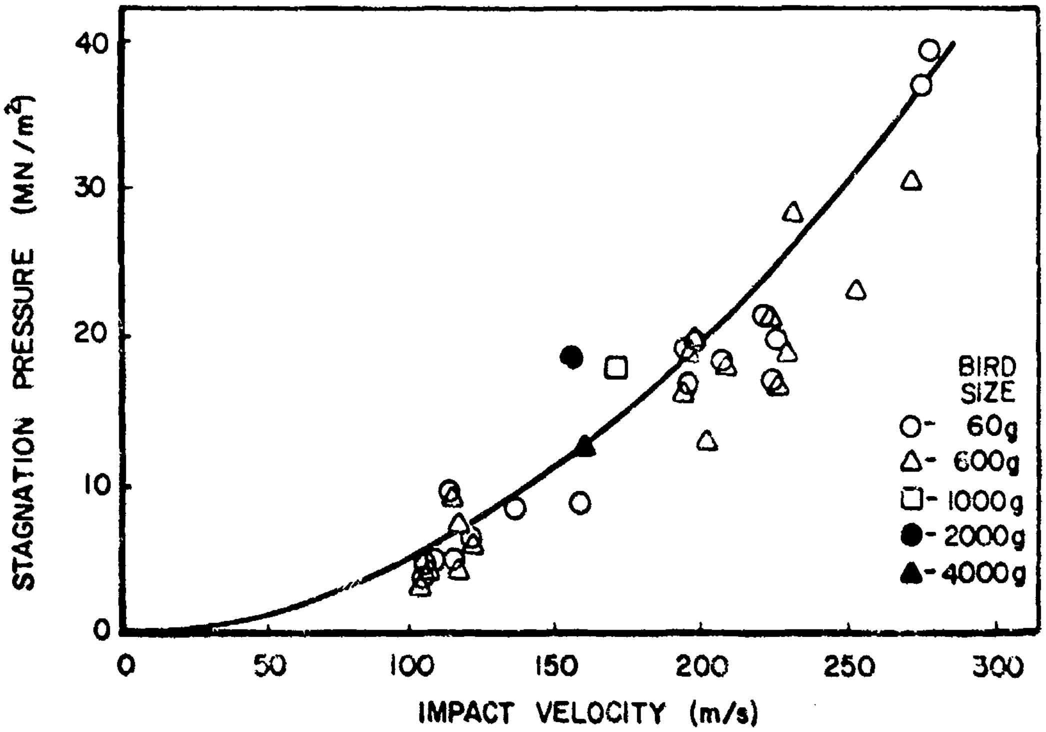

Figure 32. Steady flow pressures versus impact velocity at center of impact for normal (90°) impacts.

bird (60 g) and medium size (600 g) birds. The limited large bird data also shows good agreement.

The off-axis steady pressure data was normalized to the theoretical stagnation pressure. The results are averaged and are displayed in Figure 33. The large error bars on the mean values of pressure are indicative of the scatter in the data. This scatter is most probably due to lack of cylindrical symmetry in real birds and to real variations in bird properties from bird to bird. The mean values agree reasonably well with the steady flow predictions from Section 3.2.3.

There appears to be an experimentally significant difference in pressure distribution between medium size birds (600 g) and the small birds (60 g). There was insufficient large bird data (1 kg and above) to establish meaningful average values for the pressure distribution.

The results for oblique impact were treated in the same manner as the normal impact case. The measured pressures were normalized to the full stagnation pressures (the pressure coefficient). Pressures were measured along the major axis of the impact and along the minor axis (as shown in Figure 27). The results for the major axis are shown in Figure 34 and for

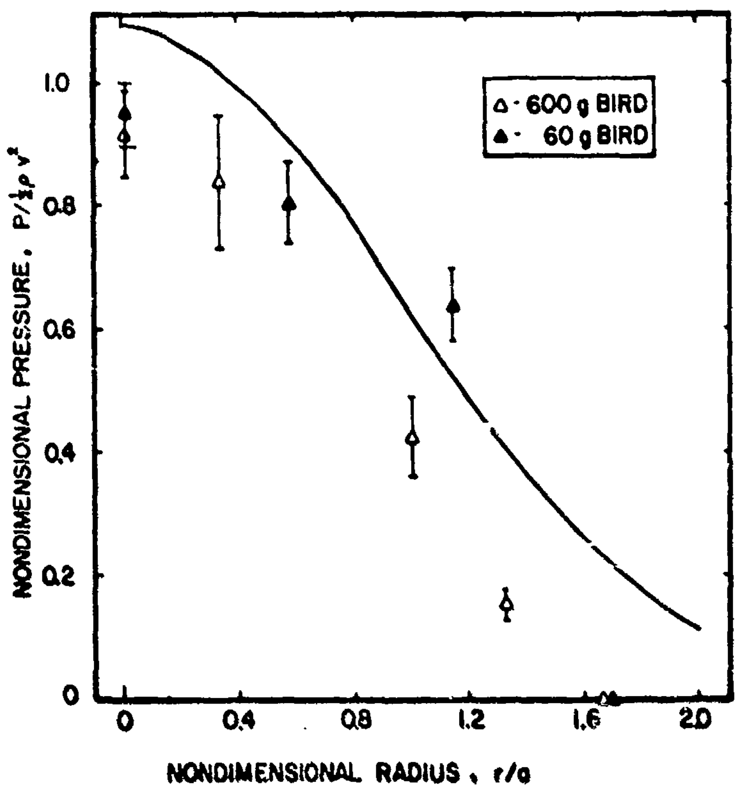

Figure 33. Steady flow nondimensional pressure distribution for normal impacts.

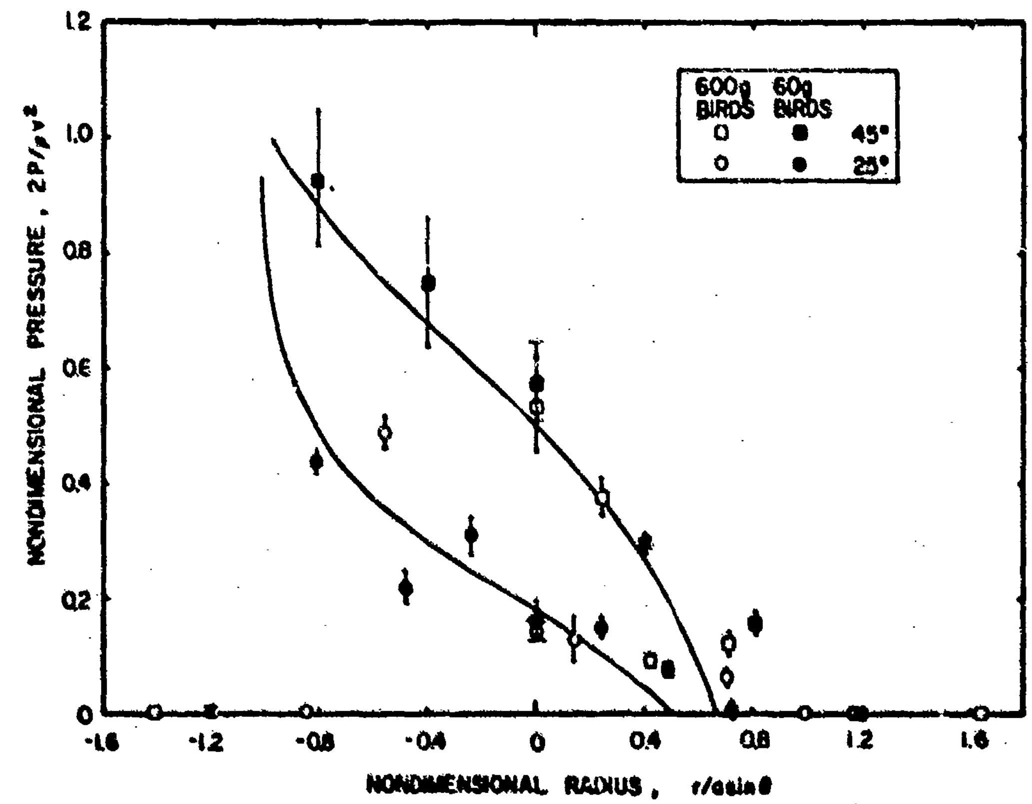

Figure 34. Steady flow nondimensional pressure distribution along the major axis for oblique impact.

the minor axis in Figure 35. Also shown on the figures are the theoretically predicted distribution (pressure coefficients) as described in Section 3.2.3.2. The agreement between the predictions and the measured values is very good over the central portions of the flow. Near the edges (nondimensional radius of one) the agreement is not so good. The potential flow solution does not adequately model the vorticity effects at the edges. However, the leading edge effects are probably of secondary importance in structural modelling and the potential flow model described in Section 3.2.3.2 should provide an extremely good prediction of the steady flow regime of bird impact. Further work on the theoretical model should be conducted to incorporate vorticity and compressibility effects.

There are very significant differences in the pressure distribution for the two angles. At 45° the full stagnation pressure is reached, while at 25° the maximum pressure for both cases occurs very close to the edge of the bird (nondimensional radius of one). The theoretical results (Figure 26) show that very little obliquity (75°) moves the stagnation point almost out to the edge. The pressure falls almost linearly from the stagnation point down to zero on the obtuse (or downstream) side of the impact. The scatter in the data is large, but there appear to be no significant measured diffferences between 60 g and 600 g bird distributions. The scatter is probably due to the effects of lack of cylindrical symmetry in the impact, small variations in bird orientation, and variations in bird properties.

3.3.4 Flow Termination

The impact pressure should return to zero when the end of the bird reaches the plate. The duration of the pressure record should thus be given by the "squash-up" time, ℓ/v. This is only true at the center of impact for normal impacts. The duration off-center and for oblique impacts can differ from the "squash-up" time depending on the exact geometry of the bird and the location of the transducer. The durations of impact pressure records were read for a number of normal impacts and the results are displayed in Figure 36. The impact duration is very close to the "squash-up" time and in agreement with the results found from Hopkinson bar testing as reported in Section II.

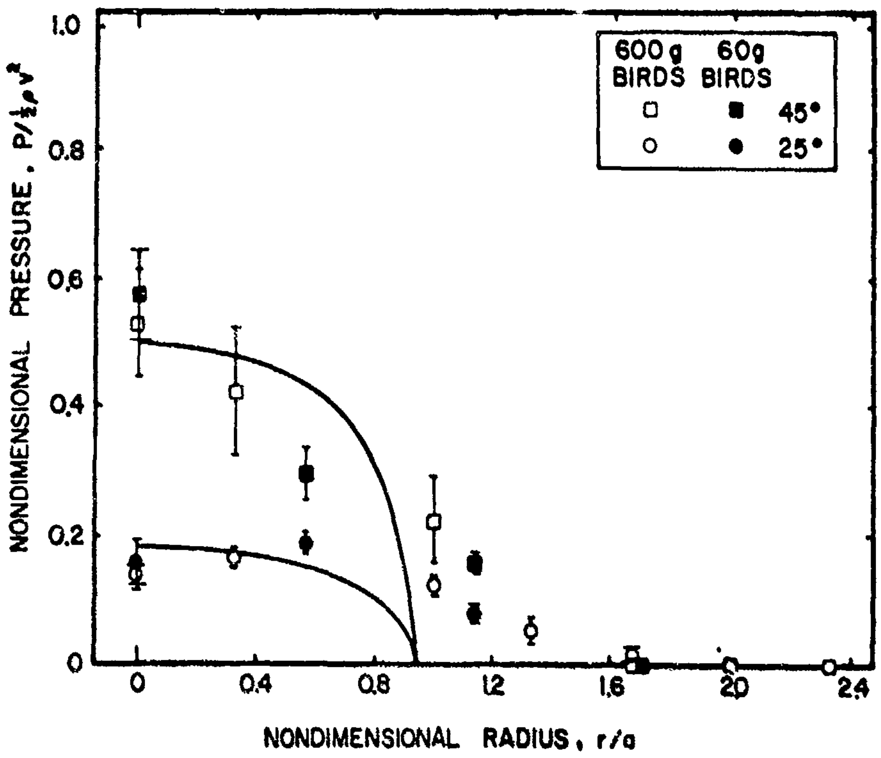

Figure 35. Steady flow nondimensional pressure distribution along the minor axis for oblique impact.

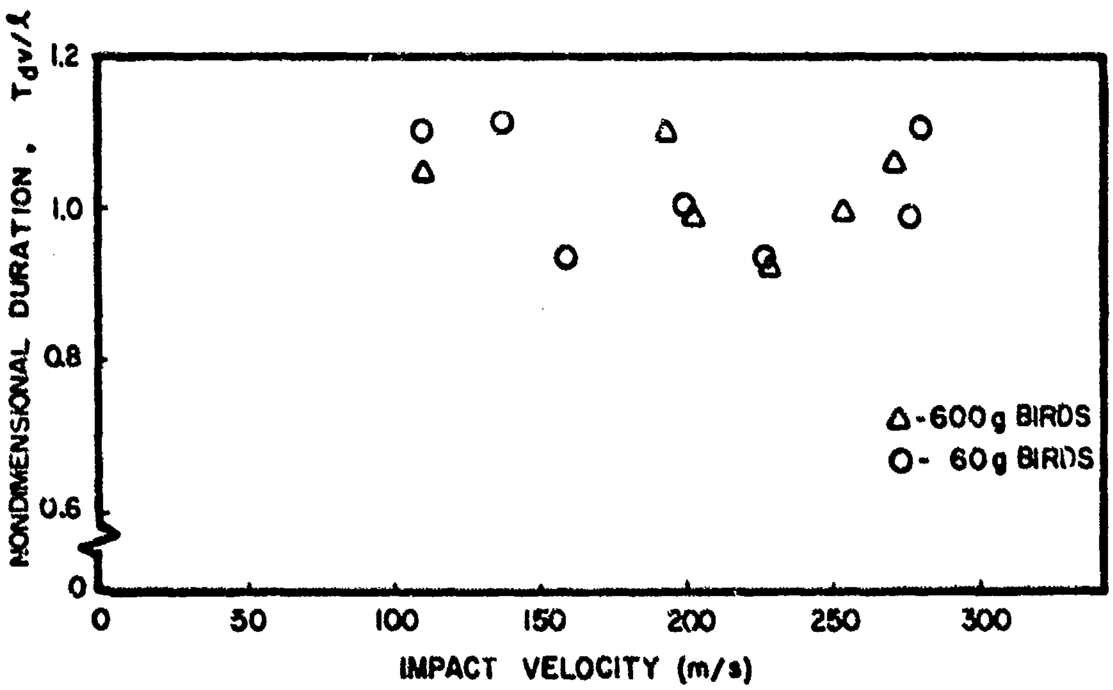

Figure 36. Nondimensional duration versus impact velocity for normal impacts.

3.4 SUMMARY

In summary, the pressure measurements indicate that birds act as a fluid during impact. The pressure records consist of an initial high pressure associated with the one-dimensional impact shock stress in the bird. This pressure decays by radial release of the high shock pressures. A steady flow regime is established providing the bird length to diameter ratio exceeds a value of approximately one. The steady pressures finally decay to zero when the end of the bird reaches the plate.

The important features of bird impact pressures can be modeled, assuming the bird has material properties described by gelatin with approximately 10 percent porosity. The impact pressures can be calculated using the Hugoniot relation ($P = \rho v_s v$) for a mixture, together with the shock properties of gelatin. In oblique impact only the normal component of impact velocity contributes to the shock pressure. Calculations of the shock release process indicate that steady flow will be established if the length to diameter ratio of the bird (in the direction of impact) exceeds approximately one. Steady flow pressures and pressure distributions can be calculated using potential flow modelling. A detailed compressible model for normal impact was developed by Wilbeck[6]. The more difficult oblique impact case was successfully analyzed using an incompressible model.

Many of the physical features of bird impact reported here were incorporated in the numerical model of Ito, et al.[4]. However, Ito, et al., use water properties for the bird model. The result is that shock pressures are too high and the decay process probably differs from real birds (which appear to have significant porosity). The steady flow regime is relatively insensitive to porosity and Ito's model should provide good results. The model reported by Ito, et al., should be expanded to include the oblique impact case as described in this report.

SECTION IV

EFFECTS OF TARGET COMPLIANCE ON BIRD LOADING

The experimental and analytical investigations reported in the previous sections of this report were concerned with bird impact onto rigid targets. The targets were not significantly moved or deformed during the impacts. This greatly facilitated the measurement and analysis of bird impact loads and such tests provided valuable insight into the bird loading process. However, aircraft transparencies are not rigid structures under bird loading. The transparency can move and deform significantly during a bird impact. It is, therefore, necessary to consider the effect that windshield response, or compliance, has on the impact loading process.

An aircraft transparency may, in general, respond to impact in two distinctly different modes which are termed locally rigid and locally deforming. In the locally rigid case the windshield does not significantly deform in the local area of impact. The process is illustrated in Figure 37. However, the windshield does translate and rotate during impact (i.e., the relative impact velocity and impact angle change during the impact process). This can result in significant changes in the impulse imparted to the windshield, the duration of the forces, the magnitude and direction of the force, and magnitude of the pressures exerted on the windshield.

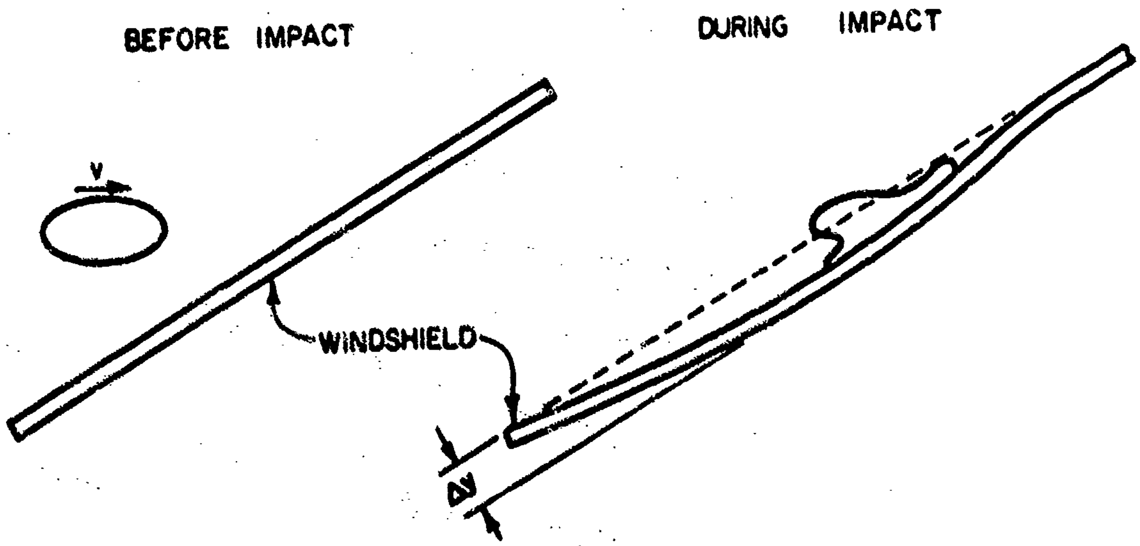

Figure 37. Locally rigid windshield response.

In the locally deforming case, the local region of impact undergoes significant deformation including local changes in angle and shape. This case is illustrated in Figure 38. The windshield forms a "pocket" around the bird. This "pocketing" behavior results in greatly increased local loading and local deformation. The phenomena displays unstable behavior; the impact force produces local deformation and the local deformation results in higher impact forces. In addition, this "pocketing" results in greatly increased momentum transfer to the windshield. This increased momentum transfer poses a threat to the structural integrity of the windshield.

The remainder of this section treats in some detail the effects of both locally rigid and locally deforming windshield response.

4.1 LOCALLY RIGID WINDSHIELD RESPONSE

In a locally rigid impact the impact velocity, impact angle, and location of impact may all change during the impact. The geometry of a locally rigid impact is defined in Figure 39. The bird is assumed to be a liquid and the center of mass is not deflected from trajectory during the impact. At some time after impact, the target surface has attained a velocity, v_p, and has displaced a distance, x, normal to the original target surface. The center of impact has displaced a distance, y, in the plane of the undeformed surface. The surface has rotated from its initial angle, Θ_i, to a new angle, Θ. The effects of these changes on various loading parameters will not be investigated.

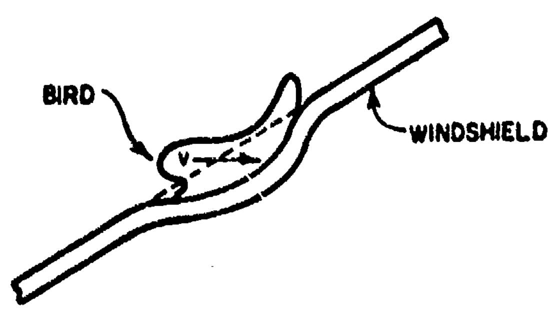

Figure 38. Locally deforming windshield response.

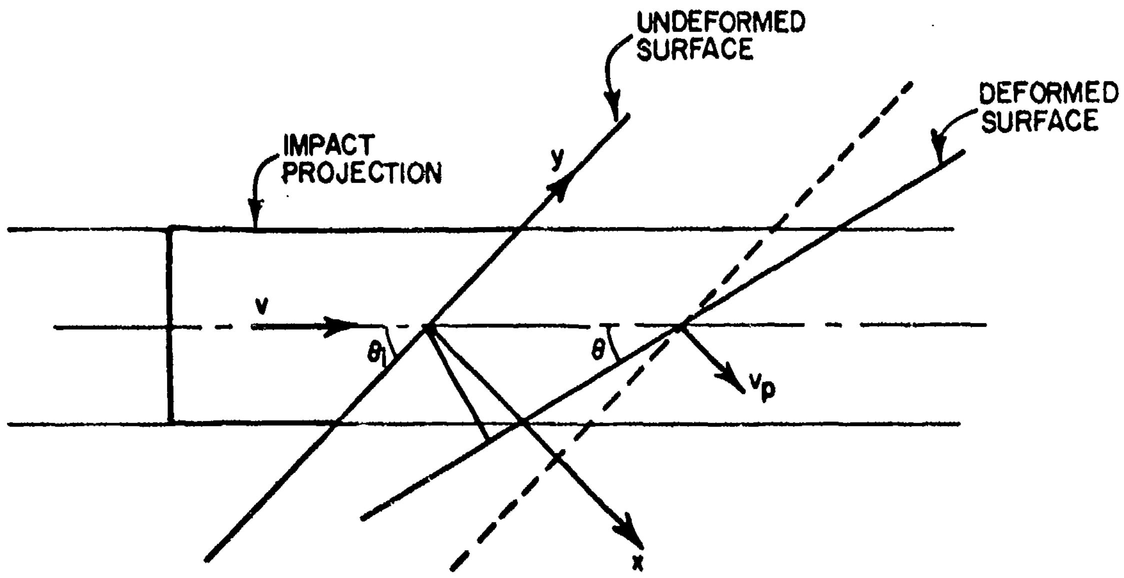

Figure 39. The geometry of a locally rigid impact.

4.1.1 The Impulse

The impulse imparted to a rigid target during impact is given by Equation (1):

$$I = mv \sin \Theta .$$

The impulse transferred to a locally rigid target can be readily deduced from Equation (1) by noting that the impulse is simply equal to the normal component of incoming momentum. In addition, it should be noted, that the impulse transfer depends only on the relative velocity between the bird and the target. Therefore, Equation (1) may be rewritten for a locally rigid target as follows:

$$I = m (v \sin \Theta - v_p) , \qquad (13)$$

where v_p is the plate velocity, or target velocity, normal to its surface. As both v_p and Θ may vary during the impact, Equation (13) is only incrementally true. To evaluate the impulse in a particular situation, Equation (13) must be expressed in differential form and integrated over the duration of the impact. The impulse cannot be specified "a priori" in a locally rigid impact.

4.1.2 The Impact Duration

In Section II it was shown that a bird behaves essentially as a fluid body during impact. The impact duration is thus given by the "squash-up" time, i.e., the time it takes for the bird to travel its own length. The duration may be thought of as the time it takes the bird to be "consumed" by the target. In a locally rigid impact, the length of bird, s, which is consumed in time, t, is given by the integral equation

$$s = \int_o^t (v - v_p/\sin \Theta)\, dt. \qquad (14)$$

Equation (14) is most easily understood by noting that $v - v_p/\sin \Theta$ is simply the relative velocity between the bird and the target along the trajectory. For locally rigid impacts the concept of nondimensional time as developed in Section II must be modified. From Equation (14) it is apparent that the "squash-up" time is simply the time at which the length of bird consumed is equal to the total length of bird available. This quantity cannot be specified prior to the impact. A more significant measure of the progress of a locally rigid impact is the nondimensional length, s/ℓ, which is given by

$$s/\ell = vt/\ell - \int_o^t (v_p/\ell \sin \Theta)\, dt \qquad (15)$$

When the plate velocity, v_p, is 0, this expression reduces to the nondimensional time as described in Section II. In a locally rigid impact, Equation (15) indicates the fraction of the bird that has been consumed at time, t, during the impact.

4.1.3 The Impact Force

With some modification, the rigid plate total force results from Section II may be applied to the locally rigid case. If the impact of the bird is considered to be a steady fluid flow process, then the instantaneous force exerted during the impact may be written as

$$F = \rho A v^2 \sin \Theta , \qquad (16)$$

where A is the cross-sectional area of the bird at any time during the impact. This assumption neglects the non-steady features of the impact, but can be adapted to include them empirically. Equation (16) applies to the rigid target impact case and may be related to the average force of Equation (4) in Section II by noting that $\rho A = m/\ell_{eff}$. Using this approach, the variation of force with time during the impact may be regarded as the variation of the cross-sectional area of the bird, A, with time during the impact. The generalized bird impact force-time profile shown in Figure 14 may then be considered as the generalized nondimensional impact area variation with time during the impact. In a previous section it was noted that the nondimensional time is better represented as a non-dimensional length in locally rigid impacts. Therefore, Figure 14 can be applied to the locally rigid impact case by recasting it as shown in Figure 40. It should be noted that Figure 40 is not intended to imply that the real variation of bird impact area with consumed length is given by this figure, but rather that the loading process can be empirically described in this manner. The nonsteady effects of impact, as well as the variations of area, are treated simply as variations of area.

Equation (16) applies to a rigid target and must be modified to properly account for locally rigid target effects. Equation (16) simply equates the force to the momentum flux incident on the target surface. The momentum flux incident on a locally rigid target surface may be derived by considering Figure 39. The relative velocity of impact normal to the target

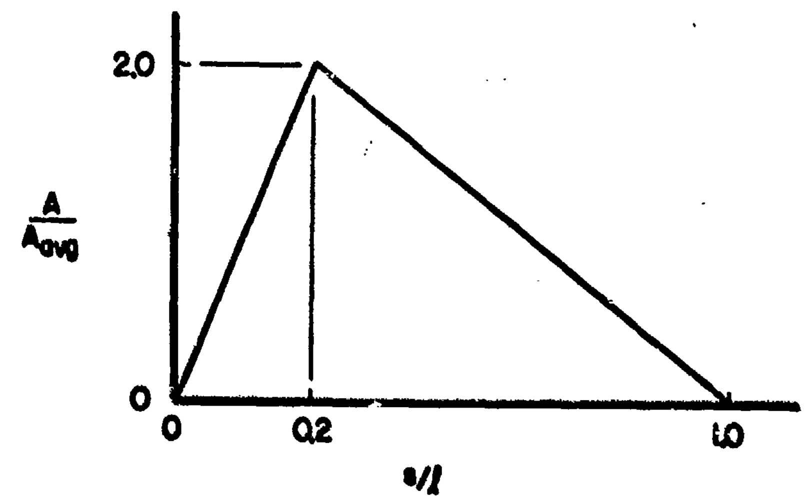

Figure 40. Nondimensional impact area versus nondimensional consumed length.

surface is $(v \sin \Theta) - v_p$. Therefore, the momentum flux at the surface is given by $[(v \sin \Theta) - v_p]^2$. This momentum flux acts on an area which is the area of the bird projected on the target surface, or, $A/\sin \Theta$. Therefore, the momentum transfer rate, or instantaneous force, exerted on the target is given by

$$F = A\,[(v \sin \Theta) - v_p]^2/\sin \Theta. \qquad (17)$$

This equation describes the force exerted on a locally rigid target during the impact. The area of the bird, A, is considered to be a function of the nondimensional consumed length as shown in Figure 40. During a calculation, the nondimensional consumed length must be continually evaluated using Equation (15). The nondimensional area (and, therefore, the actual area, A,) may then be derived using Figure 40. The area is then substituted into Equation (17) to provide the remaining unknown necessary to calculate the impact force.

The direction at which the force is applied changes continuously during the impact. However, it is always normal to the target surface and this may be readily determined during the calculation.

The location of the application of the force also changes during the impact and this can be a significant effect. As shown in Figure 39, when the target surface deflects a distance, x, the point of impact translates a distance, y. If the rotation of the target can be neglected, then:

$$y = x \cot \Theta.$$

If the target also rotates and Θ changes, then the position of impact must be computed by projecting the trajectory onto the surface of the target. In general, the position of impact will be a complicated function of displacement, x, and angle, Θ.

4.1.4 Impact Pressure

Impact pressures are modified by locally rigid target response in a manner quite similar to that of impact forces. The magnitude, direction, distribution, and location of the impact pressures are all modified by the displacement and rotation of the target surface. Each phase of the impact process, as described in Section III, is modified by the response of the target.

4.1.4.1 Shock Pressures

The initial shock pressure generated by the bird at impact is related to the shock properties of the bird and the target. The results reported in Section III were all conducted on steel targets. The impedence of steel is much much higher than that of birds. Therefore, the shock pressures reported were insensitive to the exact properties of the target. For typical windshield materials, the shock properties of the windshield can have a significant effect on the peak pressures exerted. A simple correction may be made as follows[13]:

$$P_h = \frac{\rho v_s v}{1 + (\rho v_s / {}_t v_{s_t})} \qquad (19)$$

where v_s is the shock velocity in the bird, ρ and c are the density and sound speed in the bird and ρ_t and v_{s_t} are the density and shock speed in the target. The pressure, P_h is the Hugoniot impact pressure which occurs early in the impact. As can be seen from Equation (19), as the shock impedance (ρv_s) of the target approaches that of the bird, the peak pressure approaches one-half the pressure produced by impact on a rigid target. For example, for velocities studied the shock pressure of a bird on polycarbonate is approximately 0.6 to 0.7 of the rigid target impact value. Equation (19) may be applied to oblique impacts by substituting the initial normal component of velocity, v sin Θ, for the velocity, v, and by using a shock velocity corresponding to the normal component of velocity. The target will undergo negligible gross motion during this initial stage of impact so that no further correction to peak pressure is required.

4.1.4.2 The Decay Process

The decay of the peak shock pressures during the impact will be accelerated in a locally rigid impact case. The motion of the target will provide additional release to the high pressure material. The details of the decay process cannot be specified independently of target motion. Realistic modeling of this process would have to be done using a finite difference formulation of the problem as outlined by Ito, et al[4].

4.1.4.3 The Steady Flow Regime

In the steady flow regime of the impact, the pressures are a function of the impact velocity and the impact angle. The formulation outlined in Section III can be applied to the locally rigid target case by simply substituting the relative velocity, $v - v_p/\sin\theta$, for the impact velocity, v. The distribution of pressure at any time during the impact must be calculated using the impact angle at that time. The duration of the impact must be scaled as described in Section 4.1.3, using the nondimensional consumed length rather than the nondimensional impact time.

4.1.4.4 The Termination

The pressure terminates when the nondimensional consumed length reaches one. This follows directly from the rigid impact case outlined in Section III and corresponds to the time at which the end of the bird reaches the target.

4.1.4.5 Direction and Location of Impact Pressures

The impact pressures are always applied normal to the target surface. As the target rotates during an impact, the direction of application of the pressures also changes. The location of the center of impact changes as described in Section 4.1.3 for the impact force. During computation provision must be made for the impact pressures to be relocated and redirected during the calculation.

4.1.5 Summary

For a locally rigid impact the rigid target loading models, as described in Section II and III, must be modified to account for the variation of the relative velocity, and location of the impact during the loading process. Providing the target remains rigid in the area of impact, all the important effects of target motion can be modelled as described in the preceding section.

4.2 LOCALLY DEFORMING RESPONSE

The case in which the target undergoes substantial local deformation during impact is considerably more difficult to analyze than the locally rigid case. Some features of the locally deforming case are illustrated in Figure 41. In contrast to the locally rigid case, there is gross local deformation in the region of impact. The impact angle and relative impact velocity is a strong function of position within the impact area. The flow of the bird on the target is a strong function of the exact deformation of the target. Because of this very close coupling between the loading and the response, it is probably not possible to specify the loading and

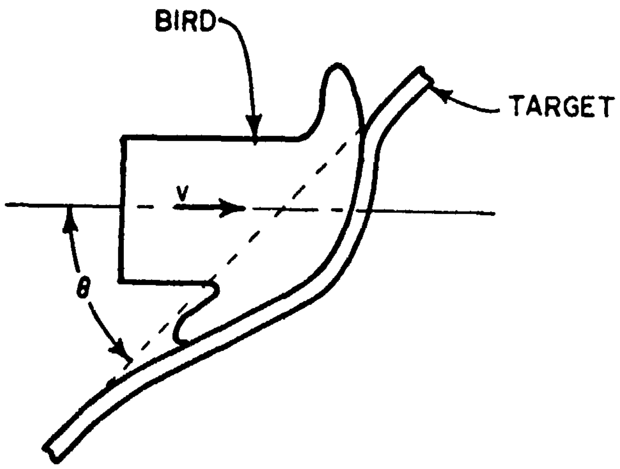

Figure 41. A locally deforming target.

calculate the response. The two processes (i.e., loading and response) are so mutually dependent that they must both be treated simultaneously in a realistic way. Such an analysis is beyond the scope of this program. However, an exploratory study of the effects of local deformation was undertaken and the results are described in this section.

4.2.1 Local Deformation Effects

The presence of local deformation during an impact would be expected to have an effect on momentum transfer, force, duration, and the rise time of the force. Local deformation would also affect pressures. However, pressures would be extremely difficult to calculate and even more difficult to measure. Attention was, therefore, restricted to impulse, force durations and rise times.

Local deformation, such as that depicted in Figure 41, results in bird material being thrown out of the impact area at higher angle than would occur had the target remained locally rigid. Therefore, the impulse transferred to the target will be greater than that which would be transferred to a locally rigid target. In addition, the direction of application of the total force is now more difficult to determine. However, it is unlikely to be normal to the original undeformed target surface. As the pocketing phenomena becomes more pronounced the momentum transfer direction will approach the original bird trajectory.

As the angle through which the bird is deflected by the local deformation increases, the forces exerted during impact might also be expected to increase. The force is a function of the average angle through which the bird is turned. As this angle increases during the impact, peak force might be expected to occur later in the impact on deformable targets than on rigid targets. Therefore, the rise time should increase. The target effectively displaces during the impact and the duration of the loading should also increase.

In summary, when compared with the rigid target loading, local deformation should increase impact forces, increase impulse transfer, increase duration, and delay the rise to peak force. To investigate some of these effects, an experimental program was undertaken.

4.2.2 Experimental Techniques

The experimental investigation of locally deforming target phenomenon is very difficult. The large elastic and plastic deformations associated with target response preclude the use of conventional instrumentation techniques such as strain gaging and pressure transducer measurements. Measurements of deformation and displacement which can be made are of limited use in investigating the loading effects of interest in this study. It was, therefore, decided to investigate the use of a Hopkinson bar technique to obtain locally deforming target loading information. The technique employed is illustrated in Figure 42. The principle of operation is identical to that described in Section 2.1. However, rather than using a bar to sense the impact force, a tube is employed. A flexible target is mounted on the tube as shown in Figure 42. The target plate is impacted centrally and permitted to deform during the impact. The loads transmitted via the plate to the end of the tube are transmitted down the tube as a strain pulse. The strain is monitored with strain gages and recorded on an oscilloscope. Using the known cross-sectional area of the tube and the modulus of the tube material, the strain-time records can be converted to force-time records. Using these records, measurements of impulse, peak force, duration, and rise time were obtained. A photograph of the tube installed on the range is shown in Figure [illegible].

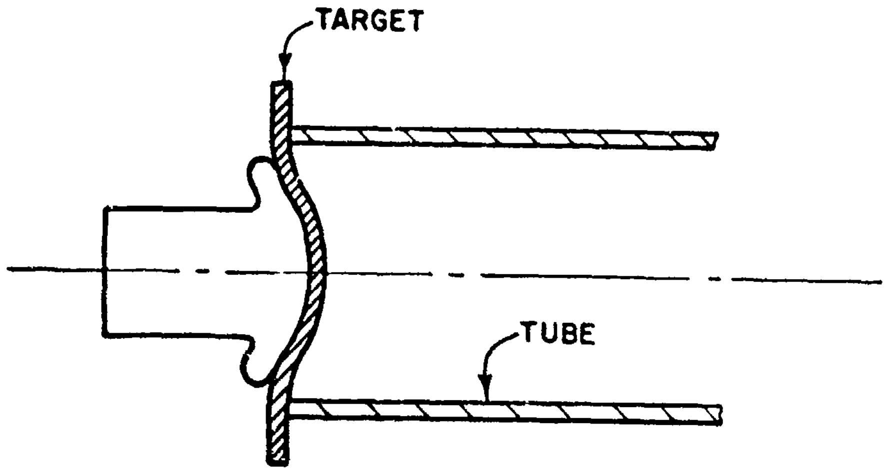

Figure 42. A Hopkinson tube.

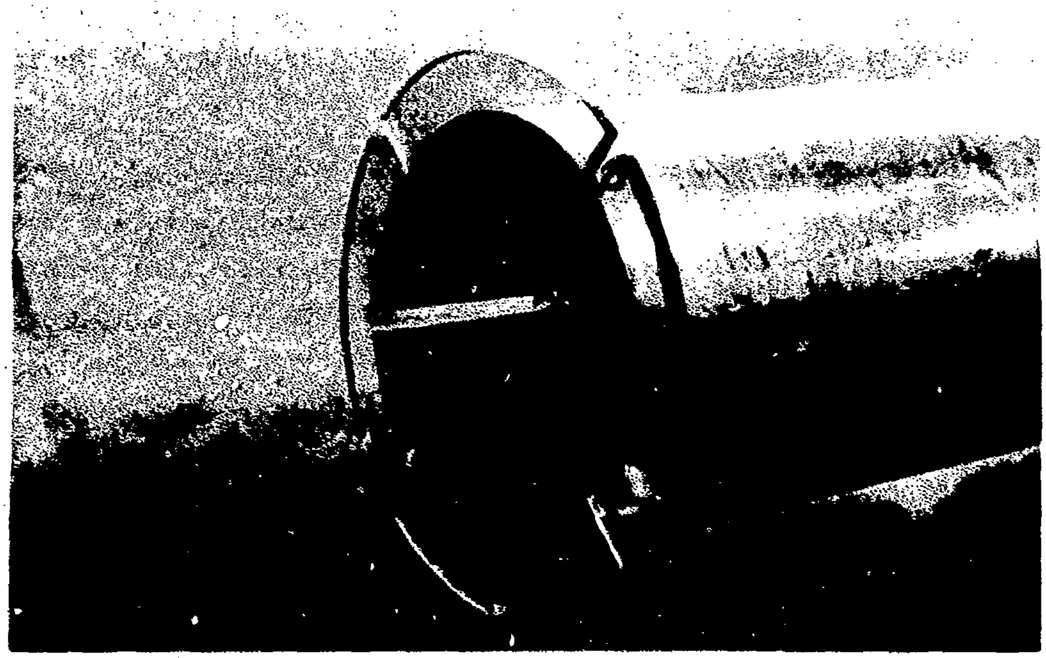

Figure 43. The Hopkinson tube in place.

The tube employed had a 15.24 cm OD and a 12.7 mm wall thickness. It was made of aluminum and was 4.87 m long. Strain gages were placed at locations 76 cm and 152 cm from the impacted end. One end was cut off perpendicular to the tube axis and used for normal impacts, the other end was cut at 45° to the tube axis and was employed for oblique impacts.

Three types of target disks were employed in the tests. A 127 mm thick steel plate was mounted on the tube to check the tube function. The steel plate acted as a rigid target. The data derived from shots on the steel plate were compared with shots on the Hopkinson bar. Two thicknesses of polycarbonate disk were tested. A highly flexible 6.35 mm thick polycarbonate disk produced very deep pocketing. A 12.7 mm thick polycarbonate disk provided intermediate flexibility.

Bird launching was conducted with the same facilities as described in Section 2.1. Due to the small size of the tube only small birds (60 g) were employed. To remove some uncertainty and ambiguity from the results, a synthetic bird material (gelatin - 30 percent phenolic microballoon) was used instead of real birds.

The displacement of the target disk was measured using a streak camera aligned across trajectory. Slots were cut in opposite sides of the Hopkinson tube to provide an unobstructed view of the rear surface of the target disk as shown in Figure 43. The dynamic displacement of the target disk during the impact was then recorded.

4.2.3 Experimental Results

A total of 63 shots were obtained on the Hopkinson tube. Of these, 14 were conducted against rigid target disks to test the tube operation. These tests demonstrated that the tube behaved as a conventional Hopkinson bar. Twenty-seven impacts were conducted against 6.35 mm thick polycarbonate disks and twenty-two against 12.7 mm thick polycarbonate disks. Strain data was recorded and converted to force data. Impulse transfer, pulse duration, peak forces, and rise times were measured. Streak records of disk motion were obtained and measurements of displacement and times were obtained. Both 90° (normal) impacts and 45° impacts were conducted.

4.2.3.1 Normal Impact Results

Normal impacts were conducted on both 6.35 mm thick and 12.70 mm polycarbonate disks. The nondimensionalized impulse transfer is shown in Figure 44. Both the 6.35 mm thick and 12.70 mm thick polycarbonate plate results are shown. The 12.70 mm thick results illustrate the expected behavior. The nondimensional impulse transfer increased from the rigid plate value of 1.0 to a value of approximately 1.1. This implies that as the plate deforms, bird material is thrown back along trajectory and the resultant impulse transfer is greater than the incoming momentum.

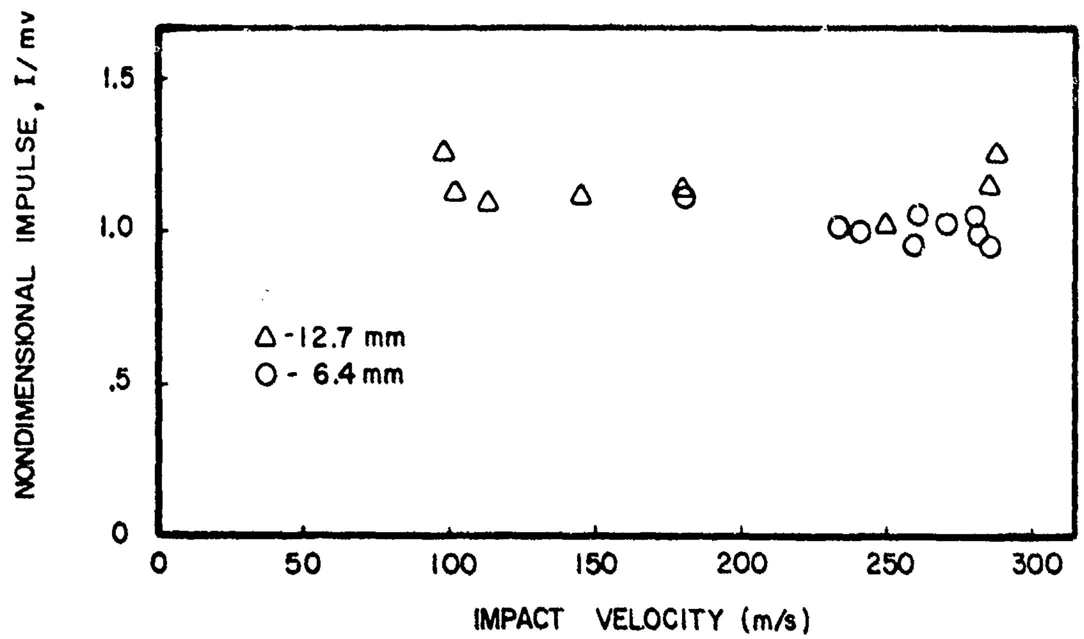

Figure 44. Nondimensional impulse transfer versus impact velocity for normal impact.

The 6.35 mm thick disk results display quite surprising behavior. The deformation of these thin disks was much greater than that for the thicker disks and the impulse augmentation might have been expected to be significantly greater than that recorded for the higher velocity tests. At high velocities the measured impulse transferred appeared to be exactly equal to the incoming momentum. The large deformation and pocketing of the plate "caught" the bird and prevented any radial flow, even at the highest velocities. The bird was recovered from these tests intact. An impact on a rigid plate at the same velocity would have completely disintegrated the bird.

For normal impact on a flexible plate, such as polycarbonate, the impact phenomena appeared to be extremely velocity sensitive. At low velocity where deformation is negligible the plate behaves essentially as a rigid plate and the nondimensional impulse transfer is approximately one. As the velocity increases, plate deformation becomes important, bird material is thrown back along trajectory and the impulse transfer is augmented. As velocity is increased further and pocketing becomes more ronounced, the bird is "caught" and impulse transfer once again returns to simply the impact momentum. If impact velocities were increased, perforation would occur and momentum transfer would drop.

The nondimensionalized duration for both 6.35 mm thick and 12.70 mm thick plates is displayed in Figure 45. There appears to be no significant difference between the thin and thick plates. At low velocity the nondimensional pulse duration is very close to one, the value for a rigid plate. However, as velocity increases, the pulse duration increases to a value of over two. The deformation of the plate has lengthened the time of application of the force by a factor of over two.

The peak force was measured and nondimensionalized as described in Section II. The results are displayed in Figure 46. At low velocities the nondimensionalized peak force is approximately 2.5 for both the thin and thick plates. This value is slightly higher than the rigid plate results recorded in Section II. However, the rigid plate results also displayed a trend to higher values at low velocities. At high velocities rigid plate results indicated a nondimensional peak force of approximately 2.0. The flexible plate results displayed in Figure 46 show a marked drop in the nondimensionalized peak force at high velocities. The thin plate values dropped to approximately 0.9 at 250 m/s while the thick plate results dropped to approximately 1.4 at 250 m/s. These values are significantly below those for rigid plates.

The rise time of the peak force was also measured and nondimensionalized as described in Section II and the results are displayed in Figure 47. At low velocities the rise time is close to that reported for rigid plates (i.e., ~ 0.2). As the velocity is increased an abrupt increase in the rise time occurs at ~ 250 m/s for thin plates and at ~ 275 m/s for the thick plates. Values of the nondimensionalized rise time at high velocities exceed one. The deformation of the target disk, therefore, delays the generation of the peak force and lowers its magnitude.

As the displacement was obviously affecting the generation of the peak force, a comparison of the rise time of the force to the time to peak displacement was made. The results are shown in Figure 48. The thin plate results show that at the higher velocities the rise time begins to increase. Presumably at sufficiently high velocities peak force will occur at maximum displacement and the rise time will be equal to the time to peak displacement. The thicker plate results do not display this trend even at the highest velocities tested. This is consistent with the lower deflections obtained with the thick plates.

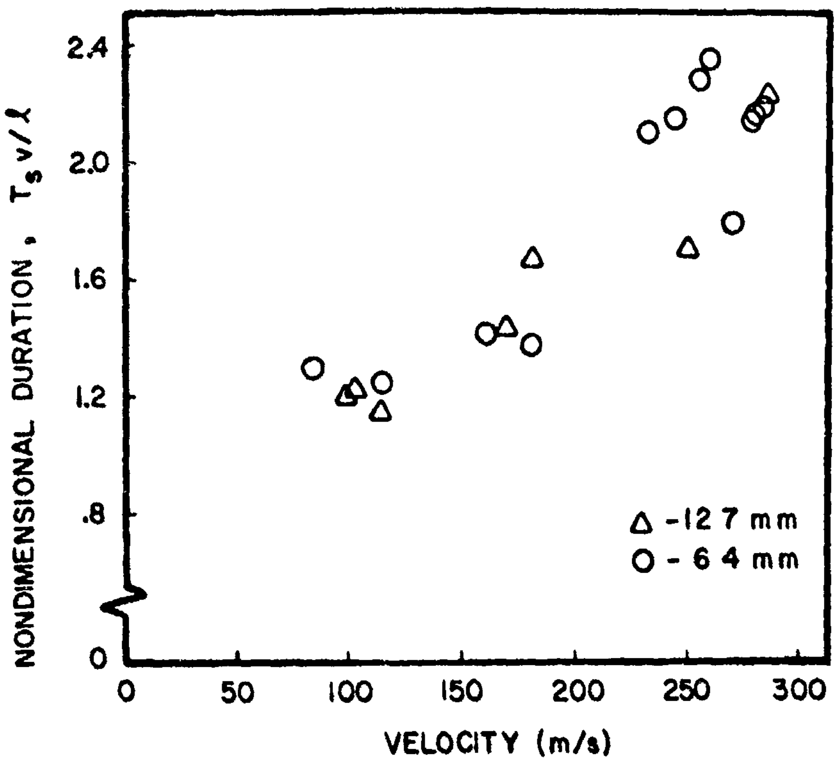

Figure 45. Nondimensional impact duration versus impact velocity for normal impact.

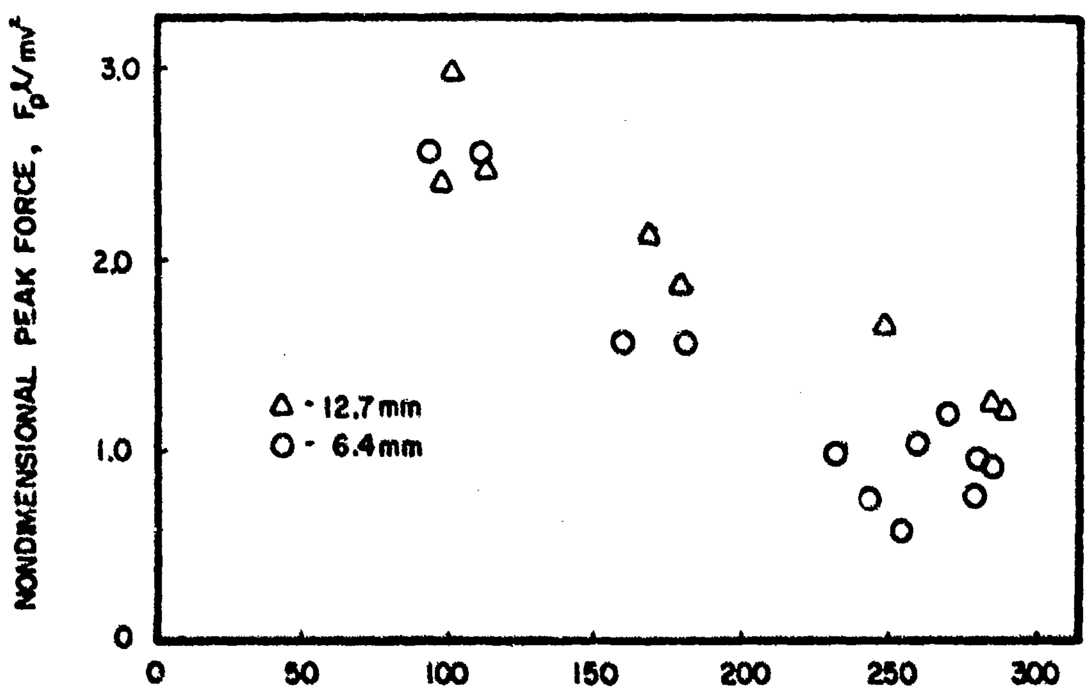

Figure 46. Nondimensional peak force versus impact velocity for normal impact.

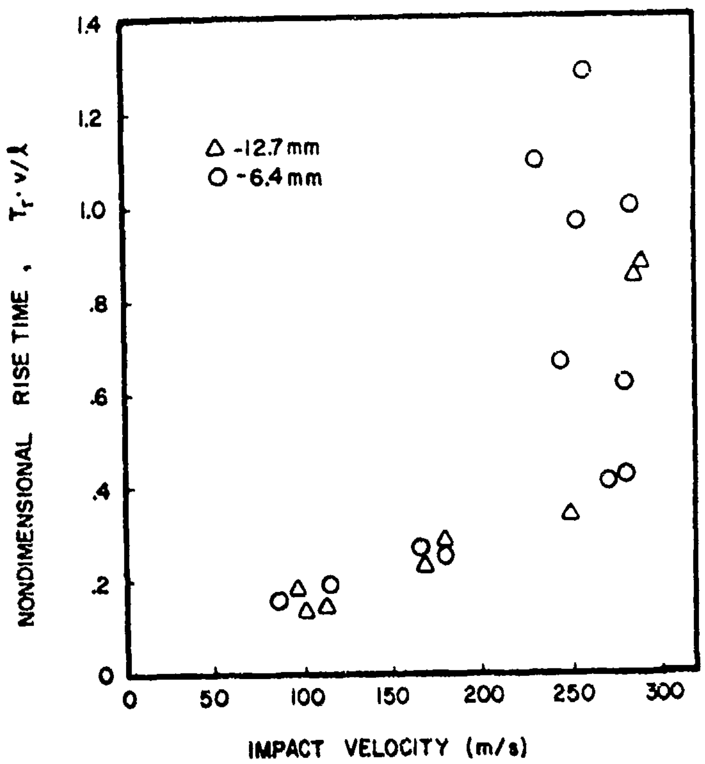

Figure 47. Nondimensional rise time versus impact velocity for normal impact.

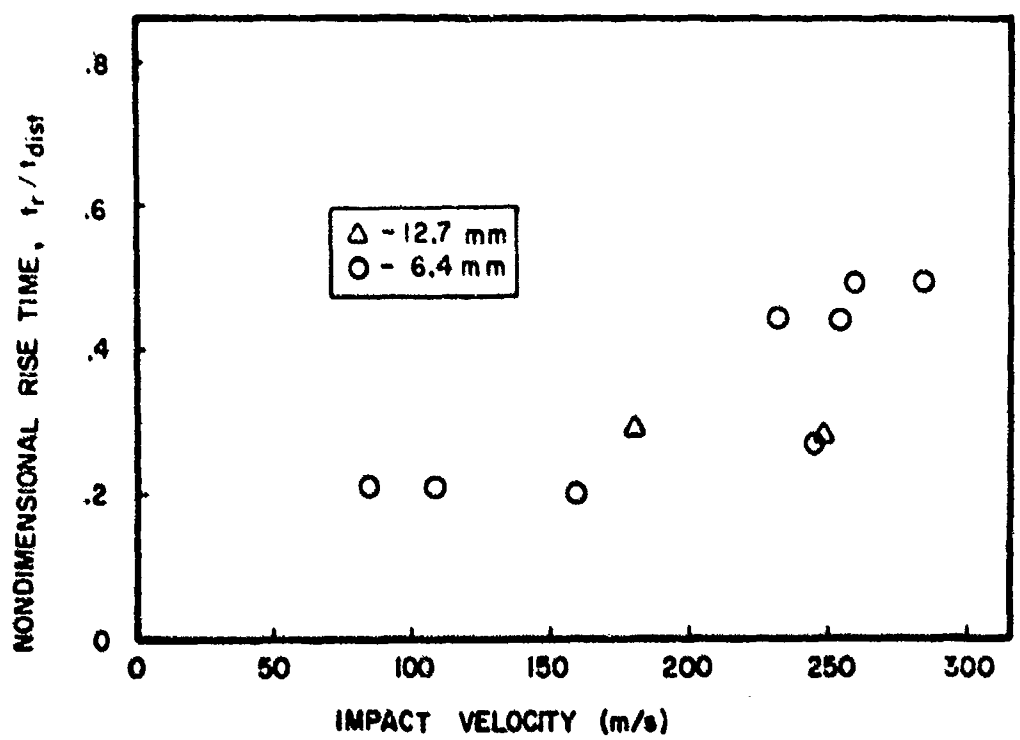

Figure 48. Rise time divided by the time to peak displacement versus impact velocity for normal impact.

4.2.3.2 Oblique Impact Results

Nine oblique impacts were conducted against the 6.35 mm thick polycarbonate disks using a sliced Hopkinson tube. The strain-time records were converted to force-time records and integrated to provide the impulse transfer. The results are shown in Figure 49. There is considerable scatter in the data which is most probably due to high order strain propagation modes excited in the tube by the highly oblique impact. However, the trends are quite clear and somewhat surprising. For high impact velocities the impulse transfer appears to be equal to the entire impact momentum of the projectile. This is a factor of two higher than what would be expected for a rigid target impact at 45°. At lower velocities there does appear to be a trend towards the rigid plate results as might be expected.

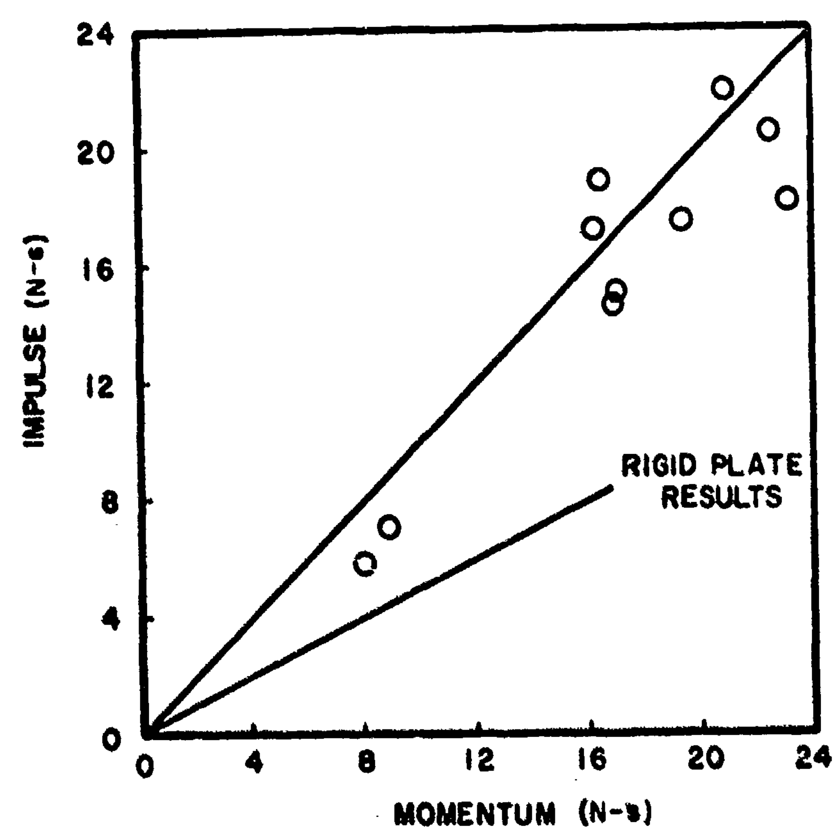

Figure 49. Impulse transfer versus impact momentum for 45° impacts.

Two mechanisms could be responsible for this remarkable impulse augmentation. The first mechanism might be that which was observed for the normal impacts, i.e., deep pocketing of the target which results in "catching" of the bird. A second mechanism could arise from deformation of the target. This would result in bird material flowing off the target surface perpendicular to the original trajectory.

Measurements of pulse duration were made and nondimensionalized as described in Section II. The results are displayed in Figure 50. As might be expected, at low velocities the nondimensionalized pulse duration is very close to the rigid plate value of one. However, at high velocities the nondimensionalized pulse duration increases to a value of over two at 275 m/s. The oblique impact records are very similar to that displayed for normal impacts and shows that target deformation significantly lengthens the duration of the impact.

Measurements of peak force were obtained and normalized as described in Section II. The results are displayed in Figure 51. Again, at low velocities the nondimensionalized peak force is very close to the rigid plate value of two. As the velocity increases the nondimensionalized peak force drops to a value of about 0.9 at 275 m/s. The oblique impact results are very similar to the normal impact results and illustrate that the target deformation reduces peak force exerted on the target.

The rise time of the peak force was measured and nondimensionalized as described in Section II. The results are plotted in Figure 52. Figure 52 shows that even at low velocities, the nondimensionalized rise time is well above that for rigid plates (0.6 as compared to 0.2). As the impact velocity is increased the nondimensionalized rise time is not so abrupt as was observed for the normal impacts. However, it reaches values which are quite similar (1.2 at 275 m/s).

The displacement of the target disk was measured and the rise time of the peak force compared to the time required to reach maximum displacement. The results are displayed in Figure 53. The oblique impact results in Figure 53 show a much stronger correlation than the normal impact results did. Even at low velocities the rise time appears to be identical to the time to peak displacement. This implies that the deformation of the target is the controlling factor in the generation of the peak force.

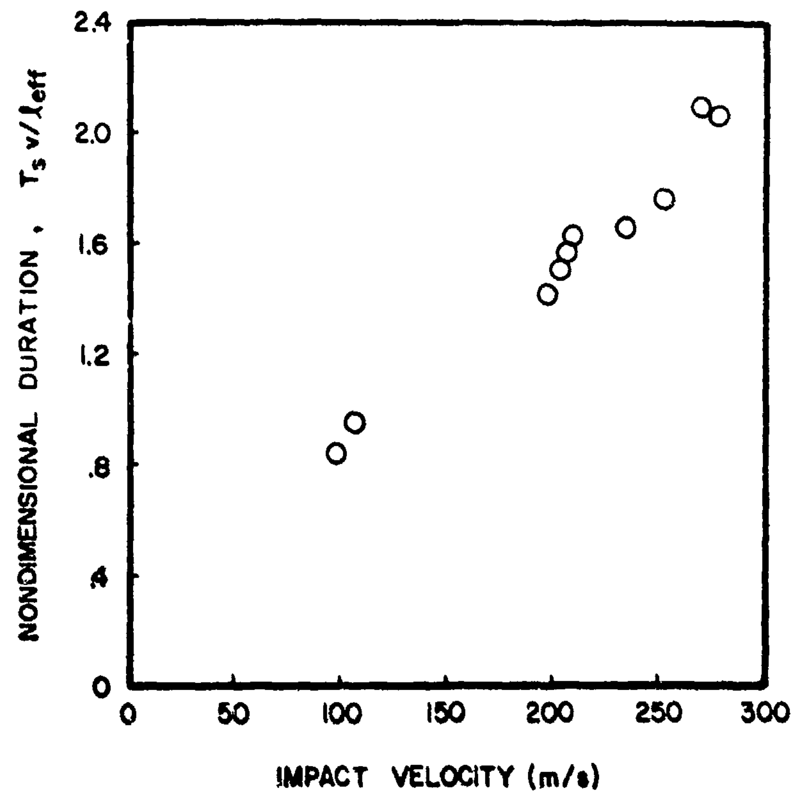

Figure 50. Nondimensionalized pulse duration versus impact velocity for 45° impacts.

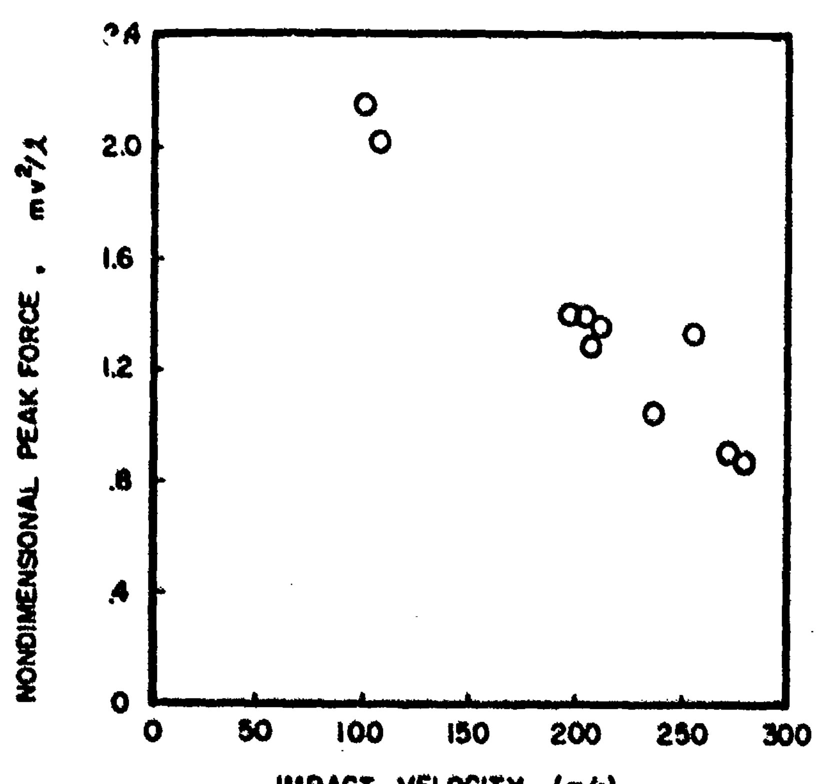

Figure 51. Nondimensionalized peak force versus impact velocity for 45° impacts.

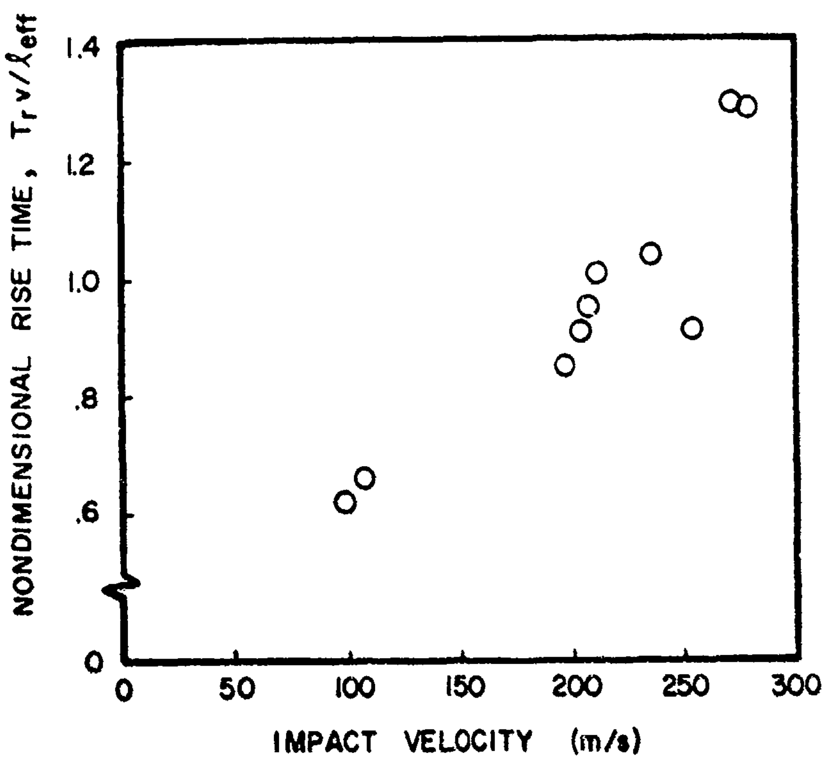

Figure 52. Nondimensional rise time versus impact velocity for 45° impacts.

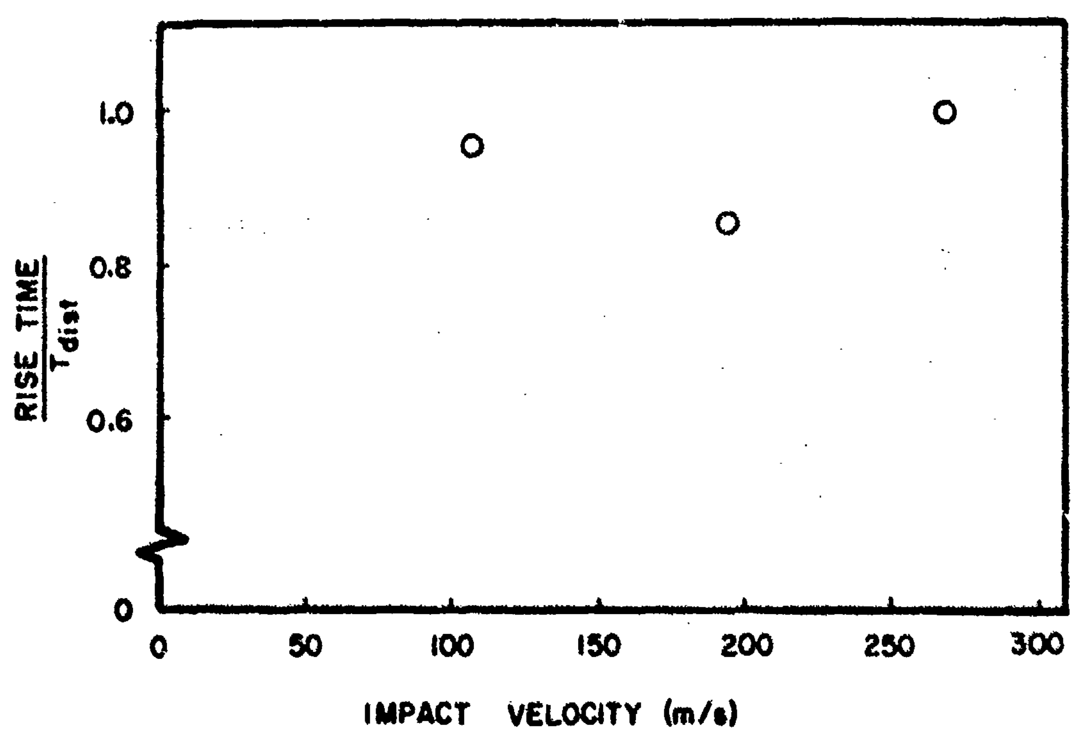

Figure 53. Rise time divided by time to peak displacement versus impact velocity for 45° impacts.

4.2.4 Summary

This series of exploratory experiments on locally deforming targets has demonstrated a number of very important features of this impact situation. Impulse transfer can be very significantly increased by local deformation of the target. This is especially true in oblique impacts where local deformation can result in the transfer of the entire impact momentum. The duration of the application of the impact force is significantly increased by local target deformation. Local target deformation produces a marked decline in the nondimensionalized peak force and a significant increase in the rise time. The impact forces are, therefore, spread out in time and reduced in magnitude by local target deformation.

SECTION V

CONCLUSIONS AND RECOMMENDATIONS

From the extensive study of bird loading discussed in this report, a number of conclusions regarding bird loading and a series of recommendations for further work have been identified.

5.1 CONCLUSIONS

From the experimental and analytical investigations conducted in this program a number of conclusions may be stated.

1. Birds behave as a fluid during impact. This is fundamentally the most significant conclusion of the investigation. The identification of the basic fluid dynamic character of the bird impact process provides great insight into the loading phenomena.

2. There are four distinct regimes of fluid flow during a bird impact. The first phase is the initial impact in which very high shock or Hugoniot pressures are generated. The second phase involves the decay of these very high shock pressures down to steady fluid dynamic flow pressures. The third phase is the phase in which the bird material flows steadily onto the target and equivalent jet flow is established. The fourth and last phase involves termination of the impact process and the return of the impact forces and pressures to zero.

3. The total force exerted by a bird at impact may be characterized in terms of the normal component of impact momentum, the duration of the impact, and the average forces exerted during the impact. These quantities may be used to nondimensionalize the important total force parameters of peak force, duration, and rise time. The nondimensionalizations derived in this study successfully scale the impact forces and account for bird size, impact velocity, and impact angle.

4. The fluid behavior of a bird during impact can be explained in terms of a roughly right circular cylindrical body composed of gelatin with a ten percent air porosity. This material model and geometry successfully predicts impact pressures, characteristic impact pressure decay times, steady flow pressures, and pressure durations.

5. Bird orientation at impact can have important effects on the loading. Angle of attack (projectile yaw) effectively lowers the length-to-diameter ratio of the bird and can affect the impact pressure decay process and the steady flow regime.

6. Target compliance has very significant and important effects on impact loads. A computational scheme to account for locally rigid target effects has been derived. Exploratory experiments on locally deforming targets have demonstrated that local deformation has very important effects on impact momentum transfer, impact loads, and impact durations.

5.2 RECOMMENDATIONS

From this work a number of recommendations for future work have been identified.

1. Large bird (1 kg and above) impact data is extremely limited. As the current standard Air Force qualification bird size is 1.8 kg for windshields, the data base should be extended to include larger bird sizes. Although bird scaling laws were identified and investigated in the current study, extension of the data base to 4 kg birds would greatly increase confidence in these scaling laws.

2. The inadvertent introduction of angle of attack into the AEDC pressure data has identified orientation as a possibly very important impact parameter. Angle of attack can increase peak and average forces by a factor of at least two while reducing durations by about the same factor. Whereas axial impacts almost always produce a regime of steady flow, side-on impacts rarely produce steady flow. The effects of orientation at impact should be more carefully and systematically investigated. An attempt should be made to determine under what conditions axial impacts are the most severe and under which conditions side-on impacts are the most severe. If side-on impacts are the most severe, under any impact conditions of interest to transparency design, then impact loads in the side-on orientation should be investigated and characterized in a similar manner to that reported here for axial impacts.

3. The development of a standard Air Force substitute bird for use in development and possibly qualification testing should be pursued. The current investigation has shown wide variation in every parameter of impact loading that was measured for real birds. These variations are undoubtedly due to real variations in bird material properties, bird structure, and bird geometry. These variations are beyond the control of the experimenter or test engineer. The demonstrated variations can be very large and represent an unacceptable and uncontrollable test variation. In contrast to real birds, the substitute bird materials that were briefly examined in this program displayed highly repeatable loading. This repeatability offers very significant advantages in the development and qualification of transparencies. Further work is required to more carefully investigate and document the properties of candidate substitute bird materials such as gelatin with ten percent air porosity. The effects of substitute bird geometry also require investigation.

4. A careful substitute validation program should be undertaken. Measurements of impact loads provide detailed knowledge of the impact process and accurate quantitative guidance in the formulation of a suitable substitute bird material and geometry. However, a careful program of substitute bird validation would be required to ensure general acceptance by the design, development, and qualification community. A series of comparison tests between real birds and substitute birds should be conducted on representative aircraft components. The damage inflicted should be quantified and compared. Such a comparison would be essential to ensure general acceptance of a substitute bird.

5. The exploratory work undertaken in this investigation on compliant targets should be extended. The formulation of the effects of locally rigid targets on impact loading should be implemented and systematically investigated. The scheme should be modeled analytically and employed to predict the impact response of a simple structure representative of a transparency. The sensitivity of the response of the structure to the details of the loading process should be investigated. In addition, the predictions of the analysis should be compared to experimentally derived values. If discrepancies occur, the source of those discrepancies should be identified. If the source is the loading model, the loading model should be appropriately modified to eliminate the discrepancy.

6. The locally deforming target investigation should be greatly extended. A detailed analysis of the Hopkinson tube specimen should be undertaken. This analysis should be used to investigate in greater detail the behavior of the target during impact. The range of phenomena which occur during local deformation should be investigated more extensively. The process of "pocketing" and the impact conditions over which it occurs should be investigated and carefully documented. The very difficult task of characterizing the local deformation and "pocketing" phenomena should be begun. The task of characterization must be complemented by an effort to reduce the characterization to useable design data and methods.

7. The theoretical analysis of oblique impact pressure distribution should be extended to include vorticity and compressibility.

APPENDIX A

LISTING OF OBLIQUE JET FLOW PRESSURE DISTRIBUTION PROGRAM

```
  2 REM BOEHMAN 2/20/77  BIRD IMPACT PROBLEM
  4 REM STEADY FLOW OF A ROUND JET IMPACTING ON AN
  6 REM OBLIQUE PLATE.
  8 READ P,N
 10 P1=P
 12 PRINT "NO. OF SOURCES=";P
 14 PRINT "NO. OF SOURCES ON Z=0 ARE";N
 18 DIM X(70),Y(70),Z(70)
 20 DIM R(70),S(70),H(70)
 22 J1=1
 23 J3=1
 24 FOR I=1 TO P1
 26 READ Y(I),Z(I),H(I)
 28 S(I)=Y(I)
 30 NEXT I
 32 PRINT "ANGLE OF PLATE (DEG)=";
 34 INPUT A1
 36 A1=A1/57.2958
 42 T1=TAN(A1)
 70 S1=SIN(A1)
 72 U6=-S1
 75 V6=COS(A1)
 82 PRINT "X-DISTANCE IS";
 83 INPUT X1
 84 J2=1
 85 PRINT
 90 PRINT "I","X","Y","YSIN(A)","Z"
 95 PRINT "U","V","W","Q","CP"
100 FOR I=1 TO P1
105 S(I)=Y(I)/S1
110 NEXT I
125 S5=S1/(2.*3.14159)
130 FOR I=1 TO N
135 IF J2>=2 THEN 150
140 Y1=S(I)
145 Z1=0.
150 U1=0.
155 V1=0.
160 W1=0.
165 FOR J=1 TO P1
166 H4=H(J)/2.
167 H3=H4/S1
170 B1=S(J)-H3
175 B2=S(J)+H3
180 C1=Z(J)-H4
185 C2=Z(J)+H4
190 D1=X1**2+(Y1-B1)**2+(Z1-C1)**2
195 D1=SQR(D1)
200 D2=X1**2+(Y1-B2)**2+(Z1-C1)**2
205 D2=SQR(D2)
210 D3=X1**2+(Y1-B2)**2+(Z1-C2)**2
215 D3=SQR(D3)
220 D4=X1**2+(Y1-B1)**2+(Z1-C2)**2
225 D4=SQR(D4)
230 IF X1=0. THEN 260
235 U2=ATN((Z1-C2)*(Y1-B2)/(X1*D3))
240 U3=-ATN((Z1-C1)*(Y1-B2)/(X1*D2))
245 U4=-ATN((Z1-C2)*(Y1-B1)/(X1*D4))
250 U5=ATN((Z1-C1)*(Y1-B1)/(X1*D1))
255 U1=U1+S5*(U2+U3+U4+U5)
260 IF ABS(Z(J))=0. THEN 335
```

```
265 D5=X1**2+(Y1-B1)**2+(Z1+C1)**2
270 D5=SQR(D5)
275 D6=X1**2+(Y1-B2)**2+(Z1+C1)**2
280 D6=SQR(D6)
285 D7=X1**2+(Y1-B2)**2+(Z1+C2)**2
290 D7=SQR(D7)
295 D8=X1**2+(Y1-B1)**2+(Z1+C2)**2
300 D8=SQR(D8)
305 IF X1=0. THEN 335
310 U2=ATN((Z1+C2)*(Y1-B2)/(X1*D7))
315 U3=-ATN((Z1+C1)*(Y1-B2)/(X1*D6))
320 U4=-ATN((Z1+C2)*(Y1-B1)/(X1*D8))
325 U5=ATN((Z1+C1)*(Y1-B1)/(X1*D5))
330 U1=U1-S5*(U2+U3+U4+U5)
335 V2=D3+(C2-Z1)
340 V3=D4+(C2-Z1)
345 V4=D1+(C1-Z1)
350 V5=D2+(C1-Z1)
355 V1=V1+S5*LOG((V2*V4)/(V3*V5))
360 IF ABS(Z(J))=0. THEN 390
365 V2=D7+(-C2-Z1)
370 V3=D8+(-C2-Z1)
375 V4=D5+(-C1-Z1)
380 V5=D6+(-C1-Z1)
385 V1=V1-S5*LOG((V2*V4)/(V3*V5))
390 W2=D1+(B1-Y1)
395 W3=D3+(B2-Y1)
400 W4=D4+(B1-Y1)
405 W5=D2+(B2-Y1)
410 W1=W1+S5*LOG((W2*W3)/(W4*W5))
415 IF ABS(Z(J))=0. THEN 445
420 W2=D5+(B1-Y1)
425 W3=D7+(B2-Y1)
430 W4=D8+(B1-Y1)
435 W5=D6+(B2-Y1)
440 W1=W1-S5*LOG((W2*W3)/(W4*W5))
445 NEXT J
450 Y2=Y1*S1
455 R2=Z1**2+((Y1+X1/T1)*S1)**2
460 IF R2>1. THEN 480
465 IF X1=0. THEN 475
470 U1=U1+U6
475 V1=V1+V6
480 Q1=U1**2+V1**2+W1**2
485 Q=SQR(Q1)
490 IF R2>1. THEN 505
495 P5=1.-Q1
500 GOTO 510
505 P5=1.-Q1
510 PRINT I,X1,Y1,Y2,Z1
515 PRINT U1,V1,W1,Q,P5
520 PRINT
525 NEXT I
530 PRINT "COORDINATES AT WHICH FLOW IS NEEDED=";
535 INPUT X1,Y1,Z1
540 J8=J8+1
545 N=1
550 GOTO 130
```

```
700 DATA 50,11
702 DATA .8,0.,.2
704 DATA .6,0.,.2
706 DATA .4,0.,.2
708 DATA .2,0.,.2
710 DATA 0.,0.,.2
712 DATA -.2,0.,.2
714 DATA -.4,0.,.2
716 DATA -.6,0.,.2
718 DATA -.8,0.,.2
720 DATA .95,0.,.1
722 DATA -.95,0.,.1
724 DATA .8,.2,.2
726 DATA .6,.2,.2
728 DATA .4,.2,.2
730 DATA .2,.2,.2
732 DATA .0,.2,.2
734 DATA -.2,.2,.2
736 DATA -.4,.2,.2
738 DATA -.6,.2,.2
740 DATA -.8,.2,.2
742 DATA .8,.4,.2
744 DATA .6,.4,.2
746 DATA .4,.4,.2
748 DATA .2,.4,.2
750 DATA 0.,.4,.2
752 DATA -.2,.4,.2
754 DATA -.4,.4,.2
756 DATA -.6,.4,.2
758 DATA -.8,.4,.2
760 DATA .6,.6,.2
762 DATA .4,.6,.2
764 DATA .2,.6,.2
766 DATA 0.,.6,.2
768 DATA -.2,.6,.2
770 DATA -.4,.6,.2
772 DATA -.6,.6,.2
774 DATA .4,.8,.2
776 DATA .2,.8,.2
778 DATA 0.,.8,.2
780 DATA -.2,.8,.2
782 DATA -.4,.8,.2
784 DATA .95,.1,.1
786 DATA -.95,.1,.1
788 DATA .75,.55,.1
790 DATA -.75,.55,.1
792 DATA .55,.75,.1
794 DATA -.55,.75,.1
796 DATA 0.,.95,.1
798 DATA .1,.95,.1
800 DATA -.1,.95,.1
*
```

REFERENCES

1. Barber, John P., Taylor, H. R., and Wilbeck, James S., "Characterization of Bird Impacts on a Rigid Plate: Part I", AFFDL-TR-75-5, January 1975.

2. Peterson, R. L., and Barber, John P., "Bird Impact Forces in Aircraft Windshield Design", AFFDL-TR-75-150, March 1976.

3. Sanders, E. J., The AEDC Bird Impact Test Facility, Air Force Materials Laboratory Report No. AFML-TR-73-126, pp 493-514, June 1973.

4. Ito, M. Y., Carpenter, G.E., and Perry, F.W., "Bird Impact Loading Model for Aircraft Windshield Design", CRT-3090-1, California Research and Technology, Incorporated, December 1976.

5. Kinslow, R., "High Velocity Impact Phenomena", Academic Press, New York 1970.

6. Wilbeck, J. S., "Soft Body Impact", Ph.D. Dissertation, Texas A&M University, May 1977, (to be published as AFML-TR-77-134).

7. Taylor, G. I., "Oblique Impact of a Jet on a Plane Surface", Proceedings of the Royal Society, Vol. 260-A, pp 96-100, 1966.

8. Milne and Thompson, Theoretical Hydrodynamics, Fourth Edition, Chapter 11, pp 283-310, Macmillan 1960.

9. Schlicting, Boundary Layer Theory, Sixth Edition, Chapter 5, pp 76-104, McGraw-Hill 1968.

10. Taylor, G. I., "Formation of Thin Flat Sheets of Water", Proceedings of the Royal Society, Vol. 259-A, pp 1-17, 1960.

11. Karamcheti, K., "Principles of Ideal-Fluid Aerodynamics", John Wiley & Sons, New York 1966.

12. Kellogg, O. D., "Foundations of Potential Theory", Dover, Incorporated, New York 1953.

☆U.S.Government Printing Office: 1978 — 757-080/146